AR-009-660

DSTO-TR-0321

DSTO

F-111C Longitudinal and Lateral Aerodynamic Flight Data Analysis for Take-off and Landing Configurations

A.D. Snowden and J.S. Drobik

APPROVED FOR PUBLIC RELEASE

DEPARTMENT OF DEFENCE

DEFENCE SCIENCE AND TECHNOLOGY ORGANISATION

F-111C Longitudinal and Lateral Aerodynamic Flight Data Analysis for Take-Off And Landing Configurations

DSTO-TR-0321

Andrew D. Snowden and Jan S. Drobik

Air Operations Division
Aeronautical and Maritime Research Laboratory

ABSTRACT

A series of flight trials was performed on an F-111C aircraft, tail number A8-132, at the RAAF's Aircraft Research and Development Unit. Data obtained from the tests has been analysed in Air Operations Division to determine the aircraft aerodynamic and control derivatives. In this report the longitudinal and lateral derivatives for the take-off and landing configurations are presented and compared with wind tunnel results.

DEPARTMENT OF DEFENCE

DEFENCE SCIENCE AND TECHNOLOGY ORGANISATION

Published by

DSTO Aeronautical and Maritime Research Laboratory
PO Box 4331
Melbourne, Victoria 3001, Australia

Telephone: (03) 9626 7000
Fax: (03) 9626 7084

AR-009-660
April 1996

F-111C Longitudinal and Lateral Aerodynamic Flight Data Analysis for Take-Off And Landing Configurations

EXECUTIVE SUMMARY

With the introduction of the variable wing sweep General Dynamics F-111C into service in 1973, the Royal Australian Air Force (RAAF) was faced with providing technical support for a range of complex systems. In particular, the aircraft has a complex adaptive flight control system which is needed to provide satisfactory flying behaviour across the aircraft's large operational flight envelope. At the time of acquisition of the F-111C, it was not possible to obtain from the manufacturers a flight dynamic model of the aircraft suitable for flight dynamic analysis. To provide these analysis capabilities a model was developed at the Air Operations Division (AOD) based on the manufacturers design data reports and from wind tunnel tests in the AOD Transonic Wind Tunnel. The model enables the investigation of the effects of pilot commands, external stores, control system modifications and atmospheric turbulence on the rigid body response.

The F-111C aircraft operated by the RAAF has a different geometry from the versions operated by the United States Air Force (USAF). The aerodynamic data supplied to Australia with the F-111C included data developed for the F-111A aircraft which has the same fuselage, and for the F-111B which has the same wing. To validate these aerodynamic data, a flight test program was conducted at the RAAF's Aircraft Research and Development Unit (ARDU) to record the flight behaviour of an F-111C in manoeuvres designed to optimise the identifiability of aerodynamic characteristics. Analysis of the data has been carried out by AOD to determine the aerodynamic characteristics.

Data from the program has been used to validate a comprehensive flight dynamic model of the F-111C which has been developed by AOD. Data from the model is currently being used in support of the F-111C Mission Simulator and Avionics Update programs to enhance the operational effectiveness of the aircraft.

Stability and control derivatives describing the longitudinal and lateral aerodynamic characteristics of the F-111C have been determined from flight test measurements. The results presented in this report are for 16° and 26° wing sweep angles in the take-off and landing configuration.

In general, all primary longitudinal and lateral derivatives show satisfactory repeatability and trends like those of the General Dynamics and AOD wind tunnel data. However, the aircraft pitch stiffness, yaw stiffness and rudder effectiveness were consistently lower in magnitude than the corresponding wind tunnel data for both wing sweeps. This is consistent with previous results for the clean aircraft configuration.

Authors

Andrew D. Snowden

Air Operations Division

Andrew Snowden graduated from the Royal Melbourne Institute of Technology in 1991, having obtained a Bachelor of Engineering Degree in Aerospace Engineering with first class honours. Before commencing work in the Air Operations Division he completed a short term attachment with McDonnell Douglas Aircraft Company, St. Louis, Missouri, as the recipient of the McDonnell Aircraft Company Aerospace Engineering Prize for 1991. He commenced employment at AOD in 1992 and has participated in several experimental investigations including the effects of the F/A-18 LEX fences on tailplane vibration and unsteady pressure measurements, and light scattering measurements in jet exhaust plumes. He currently works on the mathematical modelling of the flight dynamics of aircraft.

Jan S. Drobik

Air Operations Division

Jan Drobik commenced employment at the then Aeronautical Research Laboratories in 1978. Since graduating from the Royal Melbourne Institute of Technology in 1983, having obtained an Aeronautical Engineering Degree with distinction, he has been involved with the mathematical modelling of the flight dynamics of aircraft. He has been attached to the DSTO Salisbury S1 Wind Tunnel, working in the wind tunnel and store trajectory simulation areas (1990), and to the NASA Ames-Dryden Flight Research Facility, conducting research into aerodynamic parameter estimation (1991-1992). Mr Drobik is currently task manager of aircraft flight dynamic modelling at AOD.

CONTENTS

LIST OF TABLES

LIST OF FIGURES

ABBREVIATIONS

AEL	Advanced Engineering Laboratory
AFTRAS	Airborne Flight-Test Recording and Analysis System
AOD	Air Operations Division
ARDU	Aircraft Research and Development Unit
CADS	Central Air Data System
KCAS	Knots Calibrated Air Speed
NASA	National Aeronautics and Space Administration
NBTU	Nose Boom Transducing Unit
RAAF	Royal Australian Air Force
USAF	United States Air Force

NOTATION

a_n, a_x, a_y	(AN, AX, AY)	Normal, longitudinal and lateral acceleration (g)
b_α, b_β		Angle-of-attack and sideslip measurement bias (°)
C_A		Axial force coefficient
C_l		Rolling moment coefficient
C_m		Pitching moment coefficient
C_N		Normal force coefficient
C_n		Yawing moment coefficient
C_X		Longitudinal force coefficient
C_Y		Side force coefficient
c		Reference chord (ft)
cg		Centre of gravity
g		Gravitational acceleration
H		Altitude (ft)
I_{xx}, I_{yy}, I_{zz}		Moments of inertia about roll, pitch and yaw axes (slug.ft^2)
I_{xz}		Cross product of moment of inertia (slug.ft^2)
i		Interval counter
J		Cost function
K_α, K_β		Flow amplification factors for angle-of-attack and sideslip
	(LATSTK)	Lateral stick position (in)
	(LONSTK)	Longitudinal stick position (in)
M		Mach number
m		Mass of aircraft (slug)
n_t, n_z		Number of time history and response variables
p	(P)	Roll rate (°/s)
q	(Q)	Pitch rate (°/s)
$\bar{q}$		Dynamic pressure (lbf/ft^2)
	(RPED)	Rudder pedal deflection (in)
R		Degrees per radian (57.2958)
r	(R)	Yaw rate (°/s)
S		Reference area (ft^2)

NOTATION (continued)

T		Thrust (lbf)
t		Time (s)
u		Control vector
V		Airspeed (kn)
W		Response weighting matrix
x		State vector
$x_{a_y}, x_\alpha, x_\beta$		Longitudinal instrument offsets from cg (ft)
y_{a_y}, y_α		Lateral instrument offsets from cg (ft)
z		Measured response vector
$\tilde{z}$		Computed response vector
z_{a_y}, z_β		Vertical instrument offsets from cg (ft)
α	(ALPHA)	Angle-of-attack (°)
β	(BETA)	Angle-of-sideslip (°)
δ		Control deflection (°)
δ_a		Aileron deflection i.e. differential stabilator $(\delta_{st_R} - \delta_{st_L})/2$ (°)
δ_e		Elevator deflection i.e. symmetrical stabilator $(\delta_{st_R} + \delta_{st_L})/2$ (°)
δ_f		Flap deflection (°)
δ_r		Rudder deflection (°)
δ_{sp}		Spoiler deflection $(\delta_{sp_R} + \delta_{sp_L})$ (°)
δ_{st}		Stabilator deflection (°)
θ	(THETA)	Pitch angle (°)
Λ		Wing sweep angle (°)
$\lambda_\alpha, \lambda_\beta$		Angle-of-attack and angle-of-sideslip measurement scale factor
ξ		Parameter vector
ϕ	(PHI)	Roll angle (°)

Software Variables

Quantities listed in parenthesis indicate software notation used in time history figures in this report.

Subscripts

CADS	Central air data system instrument
CM	Crew module instrument
cg	Centre of gravity
i	Interval counter
L	Left (port)
m	Measured quantity
NBTU	Nose boom transducing unit instrument
p, q, r	Rate derivatives with respect to indicated quantity
R	Right (starboard)
$true$	True value
$\tilde{z}$	Computed response

Subscripts (continued)

α, β	Static derivatives with respect to indicated quantity
$\delta_a, \delta_r, \delta_{sp}, \delta_{st}$	Control derivatives with respect to indicated quantity
reference	Reference aircraft cg condition: longitudinal – 45%c, vertical – 177.5 in above datum waterline, lateral – on the plane of symmetry

UNITS

It is a common convention for aircraft operators to express aircraft weight, altitude, rate of ascent or descent, airspeed, and range in non SI units. These quantities are expressed in non SI units in this report in order to conform with this convention and to provide uniformity with the source data on which the results are based.

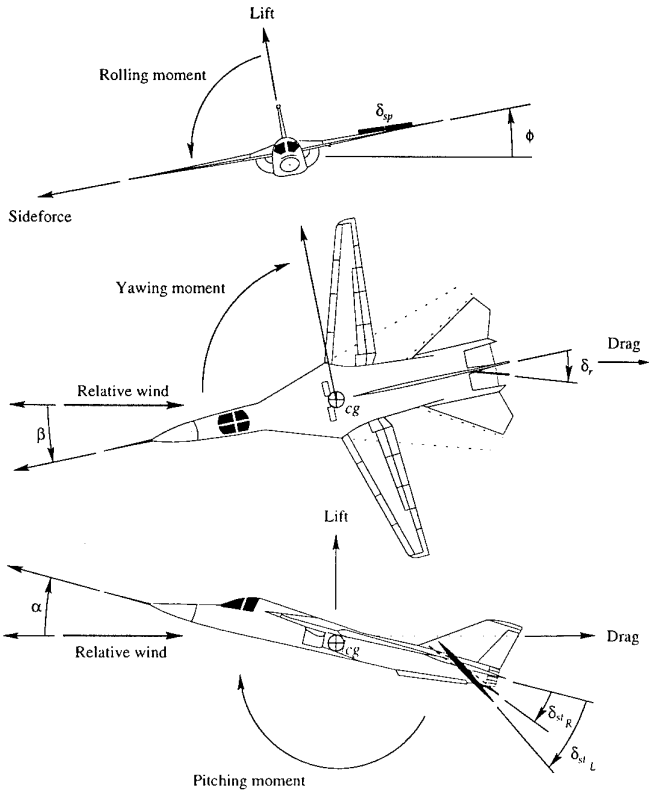

Positive forces, moments, flow angles and control deflections are shown.

Note: Positive control deflections give negative moments.

Figure 1: Force and moment convention (stability axes)

1 INTRODUCTION

The General Dynamics F-111C aircraft operated by the Royal Australian Air Force (RAAF) has a different geometry from the versions operated by the United States Air Force (USAF). The aerodynamic data supplied to Australia with the F-111C were adapted from data developed for the F-111A aircraft which has the same fuselage, and for the F-111B which has the same wing [1], [2]. To validate this aerodynamic data , a flight test program was conducted at the RAAF's Aircraft Research and Development Unit (ARDU) to record the flight behaviour of an F-111C subjected to manoeuvres designed to optimise the identifiability of aerodynamic characteristics. Analysis of the data has been carried out at the Air Operations Division (AOD) to determine the aerodynamic characteristics. Data from the program has been used to validate a comprehensive flight dynamic model of the F-111C which has been developed at AOD. Data from the model is currently being used in support of the F-111C Simulator and Avionics Update programs.

With the introduction of the variable wing sweep F-111C into service in 1973, the RAAF was faced with providing technical support for a range of complex systems. In particular, the aircraft has a complex adaptive flight control system [3] which is required to provide satisfactory flying qualities across the aircraft's large operational flight envelope. At the time of acquisition it was not possible to acquire from the manufacturers a flight dynamic model of the aircraft suitable for flight dynamic analysis. To provide these capabilities a model was developed at AOD from the manufacturer's design data reports and from wind tunnel tests conducted in the AOD Transonic Wind Tunnel. The model allows the investigation of the effects of pilot commands, external stores, control system modifications and atmospheric turbulence on the aircraft's rigid body response [4].

The installation of flight test instrumentation into an F-111C aircraft at ARDU for stores clearance testing provided an opportunity to obtain aerodynamic stability and control data. A test program was developed between AOD and ARDU and was approved in 1983. New methods of determining aerodynamic data from flight test measurements were investigated by AOD and sophisticated software for this purpose was acquired from the National Aeronautics and Space Administration (NASA) Dryden Flight Research Center. Additional analysis software was also developed at AOD. Flight testing of the aircraft was carried out at ARDU in 1987 and the analysis of the data was conducted at AOD.

This report is one of a series of F-111C aerodynamic flight data analysis reports, and presents the longitudinal and lateral stability and control aerodynamic derivatives for take-off and landing configurations. Section 2 presents details of the flight test program. Sections 3 and 4 describe the flight data processing and data analysis procedures and section 5 discusses the results of the analysis. Detailed data reduction and analysis procedures are documented in [5].

2 FLIGHT TEST PROGRAM

Testing to determine the stability and control aerodynamic derivatives was originally planned under ARDU Test Schedule 1667. The task was later redefined and conducted under Test Schedule 1691 to take into account variations in the instrumentation installation compared with the installation originally planned. Because of a delay in the manufacture of the Nose Boom Trans-

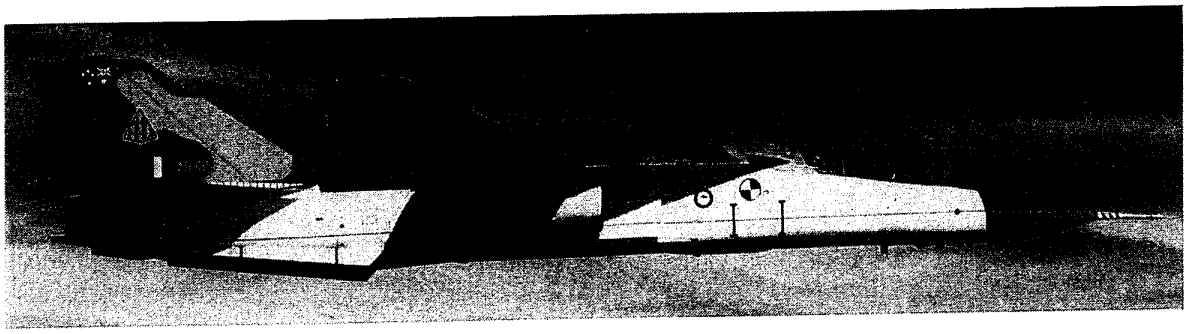

Figure 2: Instrumented F-111C aircraft (A8-132) operated by ARDU for flight trial

ducing Unit (NBTU), the flight testing was carried out in three phases. Initial flight tests, referred to as Phase 1, were conducted during February and March 1987 without the NBTU fitted. Air data and flow direction information was recorded from the aircraft Central Air Data System (CADS). The NBTU was fitted to the aircraft in September 1987. Phase 2 consisted of a number of instrumentation shakedown flights. Phase 3 testing covered additional data points together with repeated test points from Phase 1 and these were carried out in September and October 1987.

The measurement of pressure error corrections for the NBTU was carried out by ARDU as part of the Test Schedule 1691. Details of these measurements together with other details of the test program covering the aircraft, test equipment and the scope of the tests are presented in [6]. A summary of this information is included in this section.

2.1 Test Aircraft and Instrumentation

The F-111C test aircraft A8-132, illustrated in figure 2, was extensively modified under ARDU Test Schedule 1650 with the addition of flight test quality instrumentation and data recording equipment. This equipment, known as the Airborne Flight-Test Recording and Analysis System (AFTRAS), provided on-board digital magnetic-tape recording and telemetry information for real-time flight test monitoring. The instrumentation was developed for use in store-carriage and release tests and for the flight dynamic measurements. Special equipment was developed for the recording, and manual adjustment of the pitch and roll adaptive gain settings of the aircraft's adaptive control system. Due to a lack of time, instrumentation required to monitor other parts of the adaptive control system was not installed. Similarly, instrumentation for monitoring engine parameters required for detailed performance measurements was not fitted. This instrumentation was not required for the estimation of the aerodynamic derivatives, but was required for the related investigation of the adaptive control system behaviour and aircraft performance characteristics. As a result, these studies were not completed.

The NBTU used for Phase 3 of the trials was constructed by the then Advanced Engineering Laboratory (AEL) at Salisbury, and was designed to provide pitot pressure, angle-of-attack, angle-of-sideslip and linear accelerations parallel and normal to the local airflow direction. The unit was modelled on the CONRAC® Nose Boom Instrumentation Unit Model 25126F, developed by the USAF for flight dynamics and performance measurements. The NBTU is shown in figure 3 and a detailed description of the assembly is given in [7].

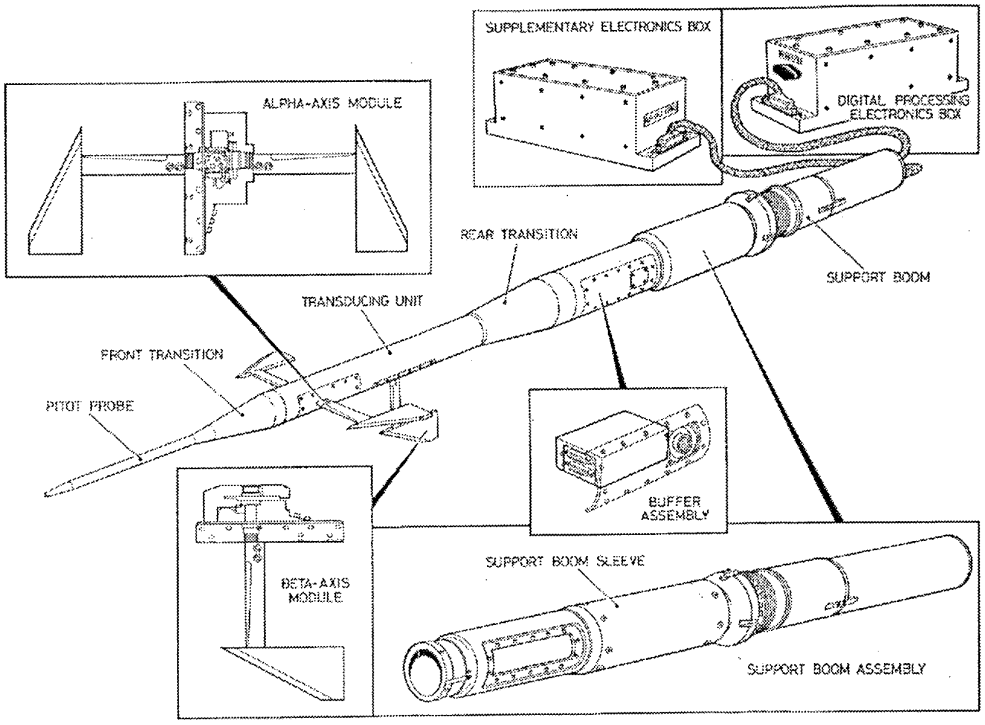

Figure 3: Nose Boom Transducing Unit (from Reference [7])

A list of the instrumentation channels (measurands), including their range and resolution [6], which were used for the flight dynamic analysis is given in table 1. Each channel was recorded at a rate of 60 samples per second.

2.2 Weight and Centre of Gravity

The test aircraft was weighed prior to the beginning of the tests and had a zero fuel weight of 50 697 lbf with the cg located at 39.9% mean aerodynamic chord for a 16° wing sweep angle [6]. During the test, the aircraft loading and cg position varied in accordance with the aircraft auto-fuel schedule. The forward and aft fuel contents gauges were calibrated prior to the test program and were manually recorded at each test point. During the test manoeuvres, the aircraft weight was typically in the region of 70 000 lbf.

2.3 Aircraft Test Configurations

In this report, results are presented for the aircraft in take-off and landing configurations for nominal 16° and 26° wing sweep angles. The take-off and landing configurations consisted of:

- landing gear down,
- wing-root glove rotated (trailing edge up),

Quantity	Symbol	Units	Range	Resolution
ACCEL LONG CG*	a_x	g	± 5	± 0.05
ACCEL LAT CG	a_y	g	± 5	± 0.05
ACCEL VERT CG*‡	a_z	g	± 10	± 0.05
ROLL RATE	p	°/s	± 300	± 3
PITCH RATE	q	°/s	± 100	± 1
YAW RATE	r	°/s	± 50	± 0.5
ROLL ACC CG	$\dot{p}$	rad/s^2	± 10	± 0.05
PITCH ACC CG	$\dot{q}$	rad/s^2	± 5	± 0.05
YAW ACC CG	$\dot{r}$	rad/s^2	± 5	± 0.05
ROLL ANGLE	ϕ	°	± 180	± 0.5
PITCH ANGLE	θ	°	± 180	± 0.5
ANGLE-OF-ATTACK*	α	°	$-3 \rightarrow 25$	± 0.5
ANGLE-OF-SIDESLIP*	β	°	± 24	± 0.5
VELOCITY	V	kn	$0 \rightarrow 900$	± 10
MACH No.†	M	–	$0.3 \rightarrow 1.3$	± 0.001
ALTITUDE†	H	ft	$-500 \rightarrow 5\,5000$	± 1.5
WING SWEEP	Λ	°	$16 \rightarrow 72.5$	± 0.05
STABILATOR (right)	δ_{st_R}	°	$-30 \rightarrow 15$	± 0.1
STABILATOR (left)	δ_{st_L}	°	$-30 \rightarrow 15$	± 0.1
RUDDER	δ_r	°	± 30	± 0.1
SPOILER (right)	δ_{sp_R}	°	$0 \rightarrow 45$	± 0.1
SPOILER (left)	δ_{sp_L}	°	$0 \rightarrow 45$	± 0.1
STICK POS (longitudinal)		in	$-4.4 \rightarrow 3.6$	± 0.05
STICK POS (lateral)		in	± 5	± 0.05
RUDDER PED POS		in	± 3	± 0.03

* NBTU measurements were also available in Phase 3
† fine and coarse readings available
‡ crew module normal accelerometer used in Phase 3 for the later part of flight 1 and all of flights 2 and 3 because of a fault with the cg accelerometer signal

Table 1: Instrumentation channels used for flight dynamic analysis

- leading-edge slats extended and
- flaps deflected (0°, 15°, 25° and 35°).

The configurations are summarised in table 2.

2.4 Flight Control System Status

The tests were conducted with the flight control system in its normal mode and with the system gains determined by the adaptive mode gain changer. However, when some manoeuvres were performed, motion due to the adaptive mode was superimposed onto the natural motion of the aircraft. In these cases, the contribution from the adaptive mode was decreased by the pilot by pumping the stick to reduce the gain.

2.5 Test Points

The matrix of take-off and landing configuration test points covered in Phase 1 and Phase 3 is given in table 2. It should be noted that the take-off and landing configuration tests were performed at a nominal altitude of 1000 ft and were thus out of ground effect.

In Phase 3, a number of Phase 1 test point manoeuvres were repeated to compare the accuracy of CADS measurements relative to the NBTU system measurements of angle-of-attack and angle-of-sideslip.

2.6 Test Manoeuvres

The following manoeuvres were performed at each test point:

1. Accurate trim.
2. Pitch input (from 1 g to approximately 2 g and return to 1 g).
3. Trim.
4. Pitch input (from 1 g to approximately 0 g and return to 1 g).
5. Accurate trim.
6. Rudder step input to left followed by aileron doublet to achieve $\approx \mp 30°$ bank angle. Rudder and aileron released together.
7. Trim.
8. Manoeuvre 6 repeated, but with rudder input to right and opposite roll applied.
9. Trim.

Manoeuvre	Phase	Speed (KCAS)	Sweep (°)	Manoeuvre Name	
				Longitudinal	Lateral
Landing Configuration					
15° flap	1	177	16	p1f6e10	p1f6e14
		188	23	p1f6e26	p1f6e30
		236	16	p1f6e01	p1f6e05
		238	23	p1f6e18	p1f6e22
34° flap	1	147	16	p1f6e50	p1f6e54
		150	20	p1f6e58	p1f6e62
	3	200	16	p3f1e72	p3f1e74
		160	26	p3f1e78	p3f1e80
Slats, no flap	1	198	16	p1f6e42	p1f6e46
		215	25	p1f6e34	p1f6e38
		240	16	p1f7e77	p1f7e81
		240	26	p1f7e69	p1f7e73
Take-off Configuration					
25° flap	1	158	16	p1f7e85	p1f7e89
	3	165	16	p3f1e84	p3f1e86

Table 2: Take-off and landing test point matrix for Phases 1 and 3, altitude = 1000 ft

Each manoeuvre is referred to by a simple naming convention as shown in table 2. Each manoeuvre has a name of the form pifjekk[x], where i indicates the Phase of the tests, j the flight number and kk the event number as recorded on the flight tape. An optional x indicates an 'a', 'b' or 'c' manoeuvre. The first longitudinal and lateral manoeuvre is referred to as the 'a' manoeuvre and the second the 'b' manoeuvre. A 'c' manoeuvre is a combined 'a' and 'b' manoeuvre.

One noticeable difference between the behaviour of the aircraft in the clean configuration and the take-off and landing configuration was the average corrected sideslip excursion. In the clean configuration this was approximately $\pm 6°$, while in the take-off and landing configuration it increased to approximately $\pm 13°$. Typical longitudinal and lateral aircraft inputs and responses are shown in figures 4, 5, 6 and 7. The effect of the flight control system is pronounced, as illustrated in figures 4 and 6, where comparisons of stick and pedal position are made with their respective control surface deflections.

3 FLIGHT DATA PROCESSING

3.1 AFTRAS Data Extraction

The AFTRAS flight data system provided procedures for accessing selected measurands, for applying calibrations to give engineering units, and for formatting the data for subsequent analysis. Calibrations were stored as polynomial coefficients and included the date of calibrations and were appended to the data files obtained from each flight. Details of these procedures are given in [8]. The procedures were carried out using program EXTRACT which was run on DEC

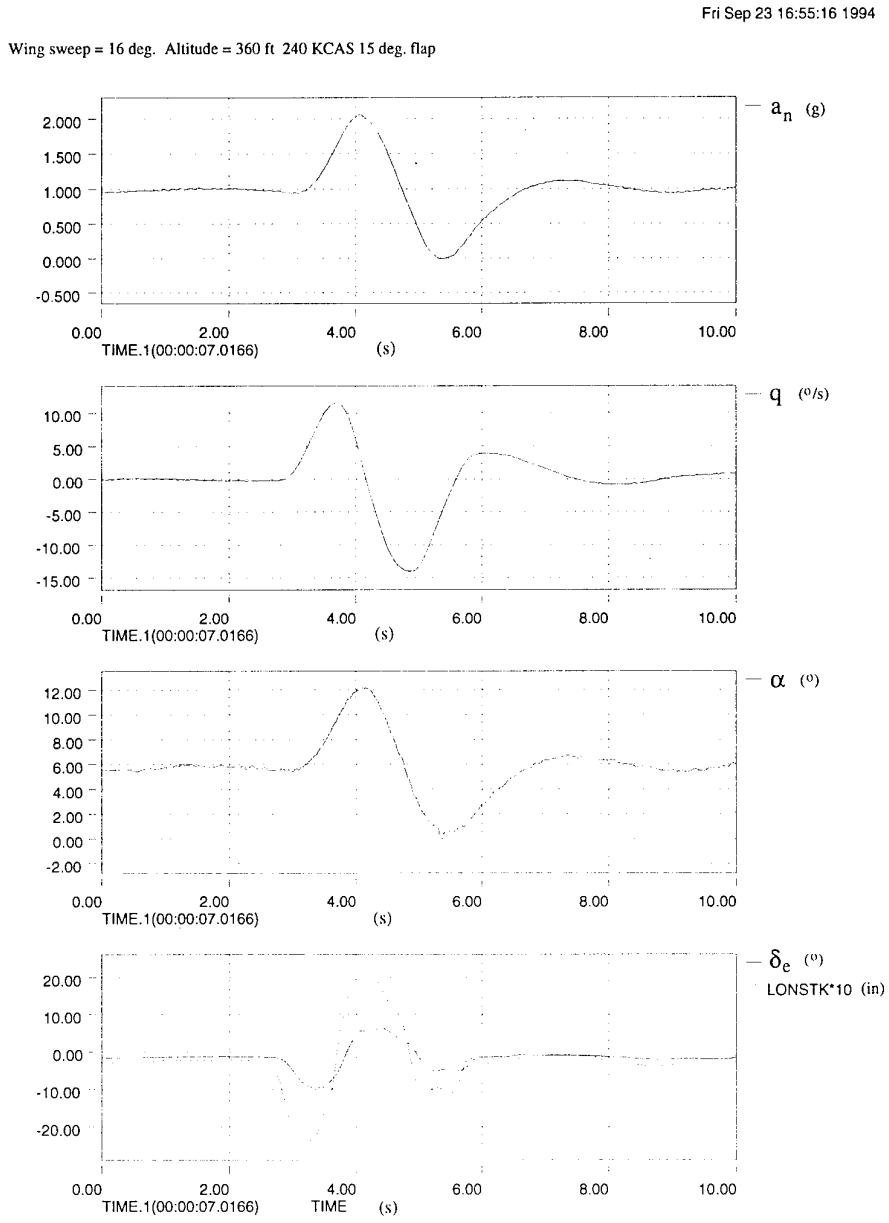

Figure 4: Longitudinal control input and aircraft response for case p1f6e01a

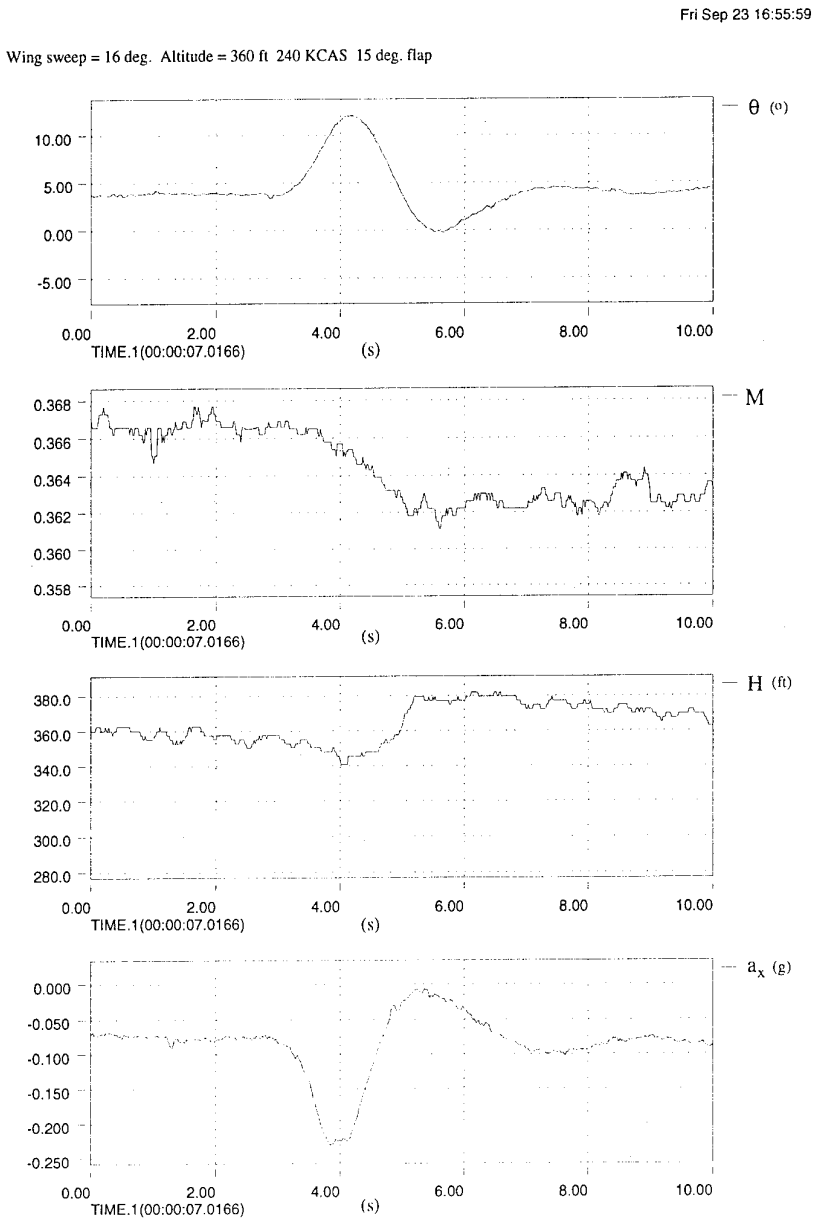

Figure 5: Longitudinal aircraft response for case p1f6e01a

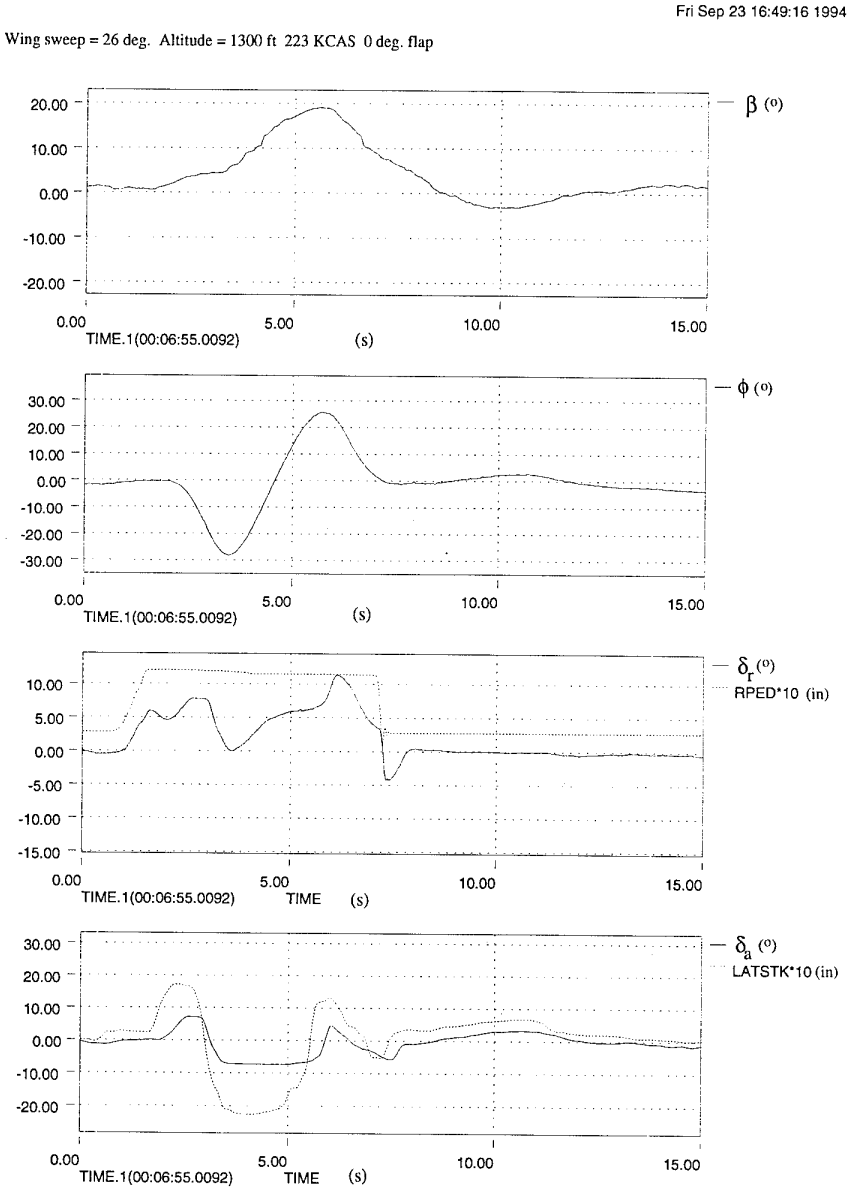

Figure 6: Lateral control input and aircraft response for case p1f6e38a

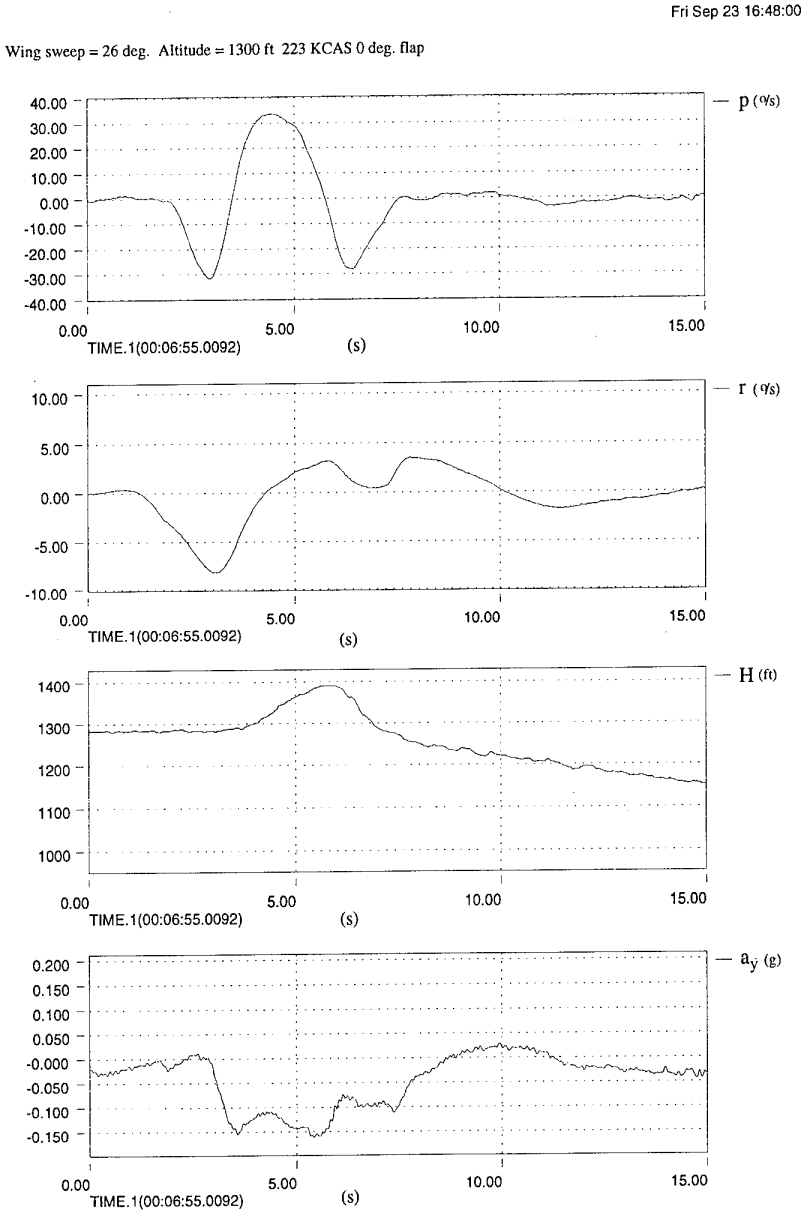

Figure 7: Lateral aircraft response for case p1f6e38a

VAX® computers at ARDU or the Aeronautical and Maritime Research Laboratory (AMRL).

3.2 Data Corrections

The techniques for determining aerodynamic parameters from the flight time histories are described in section 4. The data for input to the parameter estimation software needs additional processing for conversion to the required format and to apply measurement error corrections. This processing stage was carried out at AOD with the program FDP on an IBM UNIX ® workstation and is detailed in [5]. The operations performed were :

1. to correct the static pressure measurement for sensor position error [6], [5],
2. to adjust the airspeed and Mach number for scale altitude [5],
3. to apply time shifts to the time history records to allow for instrument, signal conditioning and recording lags (see section 3.3),
4. to adjust the angle-of-attack and angle-of-sideslip measurements for sensor location (see section 3.4),
5. to calculate elevator and aileron deflections from the measured stabilator deflections, and
6. to calculate weight, cg and inertia information from the fuel-used data.

3.3 Instrumentation Time Lags

A procedure for identifying the relative time lags between instrumentation channels was developed at AOD and is documented in [9]. This procedure uses the maximum likelihood technique and was applied to a number of selected time histories to determine the lag parameters. The resulting parameters are given in table 3 where a positive integer indicates n time samples (equivalent to a time interval of $n/60$ seconds) lagged with respect to the control deflection signals. The table shows that the NBTU signal for angle-of-attack in fact leads the control deflection signals by two sample intervals. The time lag differences, for α_{CADS} and θ, between the Phase 1 and Phase 3 flights are most likely due to changes to the instrumentation during the installation of the NBTU.

3.4 Calibration of α and β Flow Vanes

It is necessary to determine the position errors and calibration constants for the angle-of-attack and angle-of-sideslip transducers. In particular the aircraft CADS transducers were mounted close to the forward fuselage where local flow angles can differ substantially from free-stream values. A method for determining these calibration constants is described in [10]. This method uses combined parameter and state estimation techniques. The estimation software which is described in [11] and [12] was developed for AOD under a research agreement with the University of Newcastle.

Channel	Phase 1	Phase 3
δ_{st_R}	0	0
δ_{st_L}	0	0
δ_r	0	0
δ_{sp_R}	0	0
δ_{sp_L}	0	0
α_{CADS}	2	-2
α_{NBTU}	na	-2
β	0	0
θ	0	-2
ϕ	0	0
p	2	2
q	3	3
r	2	2
$\dot{q}$	na	3
a_n	4	4
$a_{n_{CM}}$	nu	0

Note: na – not available
nu – not used

Table 3: Instrumentation lags

Application of the method to the measured time histories gave estimates for the calibration constants for the CADS and NBTU angle-of-attack and sideslip measurement systems. The calculations of the angle-of-attack and sideslip vane calibration constants are described in appendices A and B respectively.

For the Phase 1 angle-of-attack sensor it was found that the calibration constant was invariant with Mach number. A constant value of 1.04 for Phase 1 was used. During Phase 3 the limited number of test cases showed that the calibration constant was not invariant with Mach number and each individual value was used in the estimation procedure.

Similar behaviour was observed for the angle-of-sideslip sensor, with a constant value of 1.55 being used for Phase 1 and the individual values for each of the three Phase 3 flights. The NBTU calibration constants are, as expected, smaller than the CADS values because the NBTU is sensing the sideslip flow angles in a relatively undisturbed flow, compared to the CADS sensor on the underside of the fuselage.

The angle-of-attack and sideslip signals must be corrected also because the vanes are not located at the aircraft cg and, therefore, aircraft rotations are incorrectly sensed by the vanes as angle-of-attack or sideslip changes. The corrections are given in appendices A and B. It should be noted that the angle-of-attack and sideslip plots in figures 4, 6, 8 and 13 are for the raw measured signal, not the corrected signal.

4 DATA ANALYSIS PROCEDURES

4.1 Aerodynamic Parameter Estimation

Several techniques have been developed in the last two decades for the estimation of aerodynamic derivatives from flight test measurements. The aerodynamic and control derivatives of the F-111C aircraft were estimated using the output-error parameter estimation technique developed at NASA Dryden Flight Research Facility [13]. This technique involves the calculation and minimisation of a cost function. The cost function is the weighted sum of the square of the difference between the computed model response and the flight measured response. The technique and associated computer program, pEst, are described fully in [14] and briefly in the following sections.

It should be noted that in [15], [16] and [17], a maximum likelihood implementation of the output-error technique was used. In this implementation, the response weighting matrix is adjusted to provide an optimally minimal cost function. The associated software, MMLE3 [18] has been replaced by pEst which has fixed weightings on the response variables. Additionally, pEst provided a far more user-friendly interface, allowing on-line interaction during the analysis as is shown in appendices C and D where example pEst runs are given for both a longitudinal and a lateral test case.

4.2 Equations of Motion

Within the range of flight conditions tested in the validation of the F-111C flight dynamic model, it has been assumed that the aircraft motion can be adequately represented by separate classical flight dynamic models for longitudinal and lateral motion. The manoeuvres have been designed so that the longitudinal and lateral motion of the aircraft may be analysed separately to give a set of stability and control derivatives describing the longitudinal and lateral aerodynamic forces and moments.

The flight dynamic model used for this purpose was the standard model described in [14] which assumes small disturbance motion and linear aerodynamic characteristics. It incorporates the non-linear equations of motion presented in appendices E and F.

4.3 A Priori Data

A priori information can be used to assist the identification process. Previous estimates of aerodynamic derivatives are often available from sources such as wind tunnel data reports. Parameter estimation results from previous similar cases may also be used to speed up convergence. In cases where a derivative makes only a small contribution to the motion, parameters may be constrained to their a priori values. The a priori values were obtained from the wind tunnel values used in the unvalidated flight dynamic model [4] discussed in section 1.

4.4 Cramer-Rao Bounds

For the unconstrained parameters the estimation procedure calculates a measure of the estimation accuracy known as the Cramer-Rao bound. The interpretation of this quantity is given in [18]. The results are plotted for each aerodynamic derivative and can be used in conjunction with the observed repeatability to indicate the estimation accuracy. To account for the fact that the measurement signal noise is bandwidth limited compared to the theoretical assumption of white noise, i.e. infinite bandwidth, the Cramer-Rao bound is factored by a multiple of 10 in accordance with the procedures described in [19].

4.5 Cost Function

The cost function is an explicit function of the computed response, and thus an implicit function of the vector of unknown parameters. The cost function used in the program is :

$$J(\xi) = \frac{1}{2n_z n_t} \sum_{i=1}^{n_t} [z(t_i) - \tilde{z}(t_i)] W [z(t_i) - \tilde{z}(t_i)]$$

where $\tilde{z}$ is the response computed by integrating the equations of motion, z is the flight measured response, ξ is the parameter vector, n_t and n_z are the number of time history and response variables respectively. W is a response weighting matrix which is defined by the user and gives an indication of confidence in each measurement.

The matches between the computed responses and the flight measured responses in the take-off and landing configuration, obtained with the default weightings, and those used for the clean aircraft configuration results, [15], [16], [17], [20], [21], [22], were poor. The aerodynamic derivatives estimated also compared poorly with the expected results. Some of the damping derivatives had the opposite sign than what was expected, incorrectly indicating that the aircraft was unstable in certain modes. Other derivatives possessed unreasonably high magnitudes. The response weightings are a function of the range of the response measured. Upon investigation it was found that the take-off and landing manoeuvres showed an increase in the range of some of the measurements compared with the clean aircraft case, e.g. angle-of-sideslip.

A scheme for establishing a new set of response weightings was therefore devised. The scheme made use of the full range of the measured response and relative confidence in each measurement response. The half range of each measured response was inverted and multiplied by 100 to give the initial matrix of weights. The factor of 100 was used solely to obtain a matrix of whole numbers. Then a confidence factor, ranging from 1.0 to 2.0, was assigned to each measured response. For example a value of 2.0 indicated high relative confidence in the measured response. The initial response weighting matrix was then multiplied by the matrix of confidence factors to obtain the final weighting matrix. Tables 4 and 5 summarise the procedure for establishing the longitudinal and lateral weighting matrices respectively. It should be noted that the lateral response weighting matrix required further refinement after preliminary pEst runs indicated less than satisfactory matches between the measured and calculated responses. The sensitivity of the resultant matches to weighting matrix variations is indicative of the low confidence in

Response	Range	Inverse*100	Confidence	Weight
α	0 to 11	18.20	1.5	27
q	$\pm$15	6.67	2.0	13
θ	0 to 15	13.00	1.0	13
a_n	0 to 2	100.00	2.0	200

Table 4: Longitudinal response weighting matrix.

Response	Range	Inverse*100	Confidence	Weight	Adjusted Confidence	Adjusted Weight
β	$\pm$10	10.0	1.5	15.0	0.75	7.5
p	$\pm$40	2.5	2.0	5.0	1.76	4.4
r	$\pm$8	12.5	2.0	25.0	3.20	40
ϕ	$\pm$40	2.5	1.0	2.5	1.60	4
a_y	$\pm$0.3	333.0	2.0	666.0	4.00	1333

Table 5: Lateral response weighting matrix.

some of the estimated parameters primarily because of the flight control system damping out the natural response of the aircraft. It should be noted that the estimated derivatives themselves are insensitive to changes in the overall weightings. Experience at NASA Dryden has indicated that doubling of the weighting should result in a 5% or less change in parameters. The purpose of calculating a new set of weightings was to obtain a better match between the calculated aircraft responses and the flight measured responses. The adjusted weighting matrix is shown in table 5.

4.6 Reference cg Correction

Longitudinal, and to a lesser extent, lateral derivatives, vary with cg position. The cg position varies with fuel usage and the flight test results were calculated at the actual flight test cg position. The wind tunnel results have been plotted with respect to the flight test cg as well as the reference cg position. The reference cg was at 45% mean aerodynamic chord, 177.5 in above the waterline and at the zero reference point laterally.

A full summary of the cg corrections is given in [23].

5 RESULTS AND DISCUSSION

5.1 Longitudinal Derivatives

For each longitudinal manoeuvre the output-error parameter estimation program, pEst, was used with the elevator deflection as input, and with the following measurands as responses :

- angle-of-attack, α,
- pitch rate, q,
- pitch attitude, θ, and
- normal acceleration, a_n.

In the clean configuration analysis [15], [16], [17], the pitch attitude was recorded but was given zero weighting in the identification process. For the take-off and landing configurations, the pitch rate data alone did not provide adequate information for the identification process. Hence the pitch attitude was also included as a response. In general, for all derivative identification it was found that the best results were obtained when the aircraft was trimmed accurately before each manoeuvre. As was shown in [15], [16] and [17], on some occasions trim was not obtained between consecutive longitudinal manoeuvres, so for these cases the two manoeuvres were analysed as one. This resulted in an overall reduction in the number of test cases. Allowing the aircraft to trim after each manoeuvre enabled an accurate 'end of manoeuvre' time to be defined. Analysing the data beyond this point resulted in a reduction in the consistency of the derivatives.

An example of the time histories is given in figure 8. The flight measured response is drawn as a solid line. The computed response is drawn as a dotted line and is also identified by the addition of `-HAT` to the name. The time history plots in figure 8 and the Cramer-Rao bounds were used to assess the accuracy of the identification procedure.

Initially, the responses were not well matched for a number of cases. The matches were improved by adjusting the response weighting as discussed in section 4.5. The normal acceleration weighting was increased significantly from the default pEst value, improving the match, and this led to a closer match between the flight estimated normal-force-coefficient derivative values and the wind tunnel results.

The pEst program calculates the coefficients in body axes. To convert to stability-axis coefficients the following relationship is used :

$$C_L = C_N cos\alpha - C_A sin\alpha$$

It should be noted that the thrust was not measured in the flight test program. Thus none of the axial force derivatives have been estimated. The error introduced by neglecting the axial force derivatives is small for low angles-of-attack. See [24] for a more detailed description of stability-axis and body-axis systems.

The longitudinal derivatives identified are given in table 6 and the results shown in figures 9, 10, 11 and 12. The derivatives estimated from the flight tests are for the actual flight cg. To

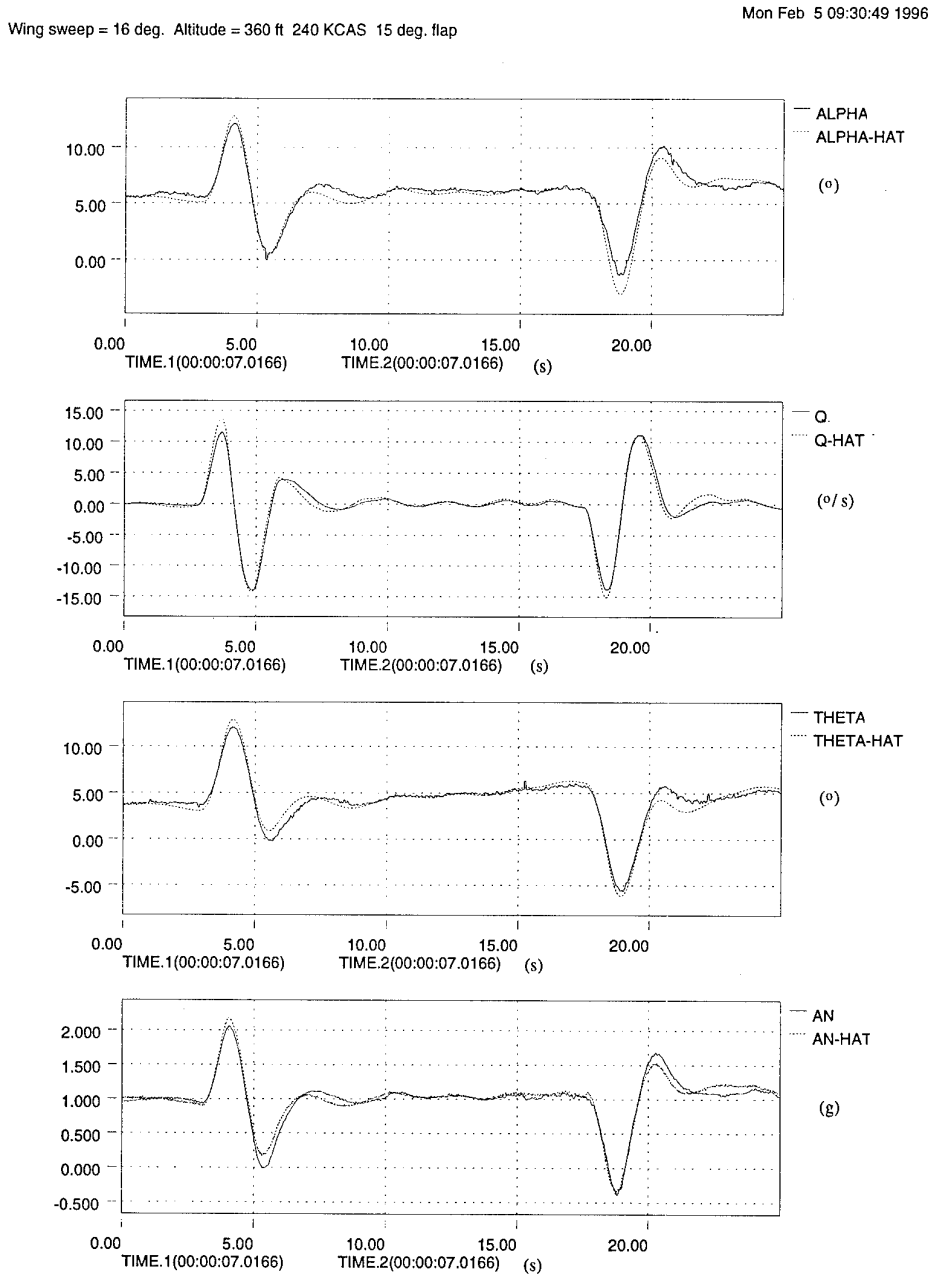

Figure 8: Longitudinal response to elevator doublet for case p1f6e01c

	Normal Force	Pitching Moment
Aerodynamic	C_{N_α}	C_{m_α} C_{m_q}
Control	$C_{N_{\delta_e}}$	$C_{m_{\delta_e}}$

Table 6: Longitudinal derivatives estimated

enable valid comparisons the wind tunnel data have been adjusted to the flight cg value. The $C_{N_{\dot{\alpha}}}$, C_{N_q} and $C_{m_{\dot{\alpha}}}$ aerodynamic derivatives used in the longitudinal flight dynamic model were not identified due to their small contribution and/or the difficulty in identification.

5.1.1 Angle-of-Attack Derivatives

Generally the C_{N_α} derivatives shown in figures 9, 10, 11 and 12 display reasonable agreement with wind tunnel results for the same flight conditions, including flap and cg position. However, the C_{N_α} value estimated for the 26° wing sweep case with 34° flap angle, shown in figure 12, appears to be poor and the large Cramer-Rao bound reflects this.

The pitch stiffness derivative, C_{m_α}, is a linear function of cg position. Figures 11 and 12 show that the estimated C_{m_α} values, for both wing sweep angles, are significantly lower in magnitude than the wind tunnel values adjusted to the flight cg and that the pitch stiffness increases with flap deflection. It should be noted that for the 16° wing sweep case the wind tunnel values of pitch stiffness at the reference cg position are unstable. This is because the reference cg is an unrealistic value for a 16° wing sweep; correcting the cg for actual flight conditions results, as expected, in a stable derivative.

5.1.2 Pitch Rate Derivatives

During the initial estimation of the longitudinal derivatives, C_{N_q} showed considerable variability when identified. The C_{N_q} derivatives estimated for the clean aircraft configuration [15], [16], [17] were in good agreement with the wind tunnel data and so wind tunnel values of C_{N_q} for the take-off and landing configuration were used as a priori data and C_{N_q} was fixed. Fixing C_{N_q} did not affect the final match nor did it cause any significant changes in the remaining estimated derivatives.

The total restoring pitching moment following a disturbance consists of contributions due to the stabilator commanded by the automatic control system as well as contributions due to pitch rate, angle-of-attack and rate of change of angle-of-attack. An ideal manoeuvre to identify the pitching moment derivatives would be a sudden stabilator (pulse type) input followed by zero input to allow the aircraft to damp naturally. Unfortunately in some manoeuvres the stabilator inputs were varying over the entire manoeuvre, due either to the pilot adjusting the stabilator position, or the aircraft control system providing artificial pitch damping. Although the identification model is still applicable in these cases, the resulting response contains little information from which to determine the pitch damping derivatives accurately. Testing with the automatic

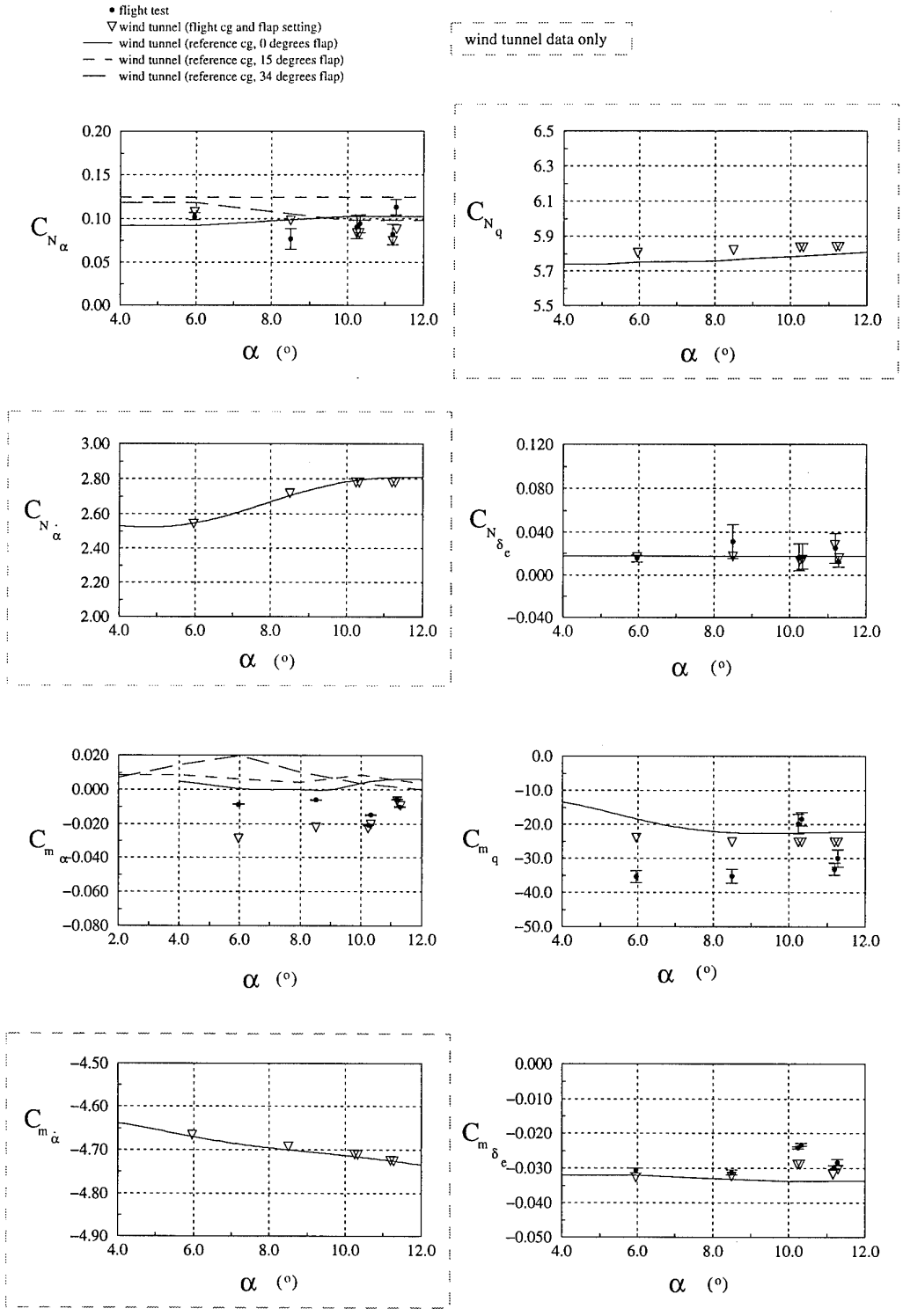

Figure 9: Longitudinal aerodynamic derivatives for $\Lambda = 16°$

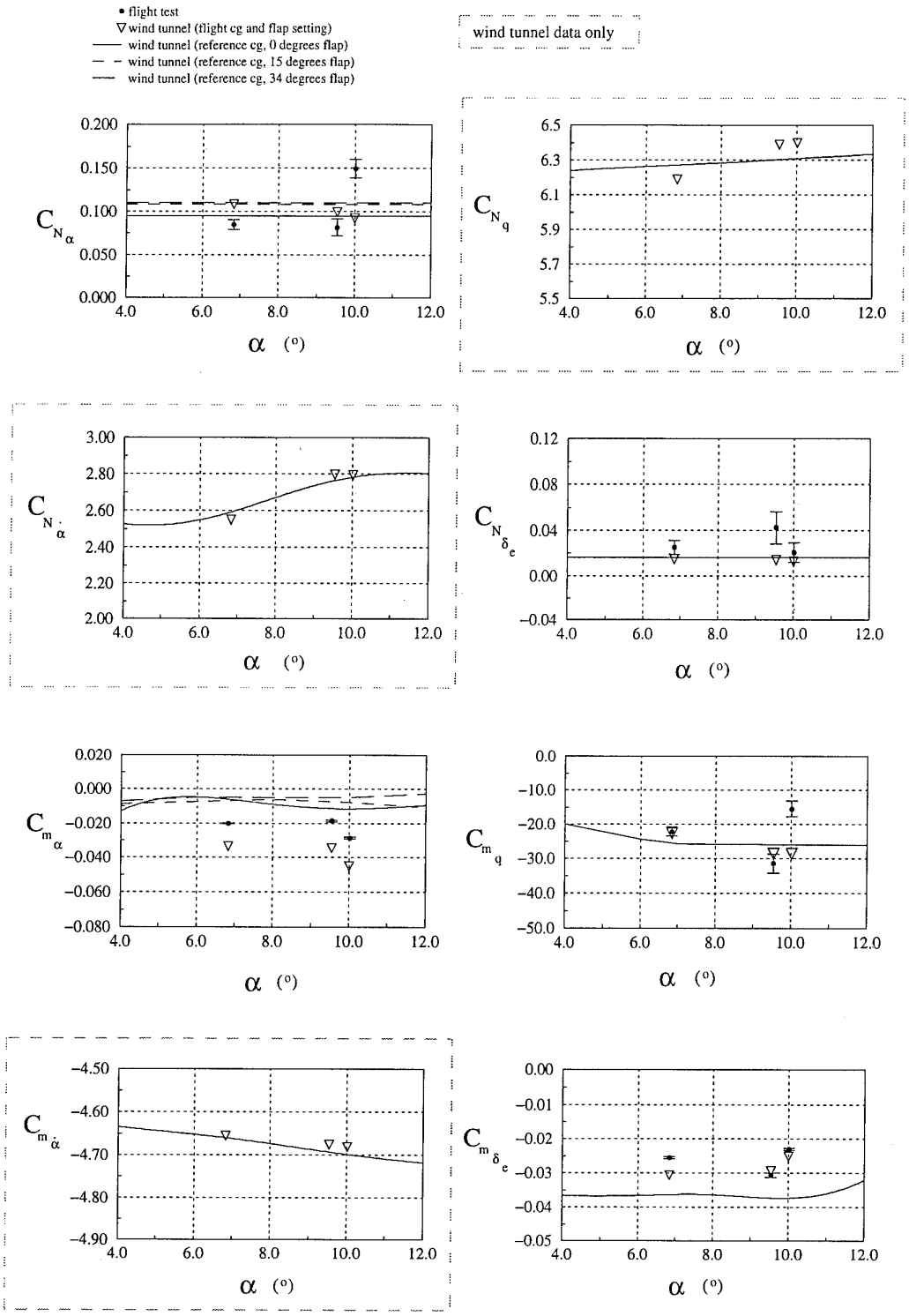

Figure 10: Longitudinal aerodynamic derivatives for $\Lambda = 26°$

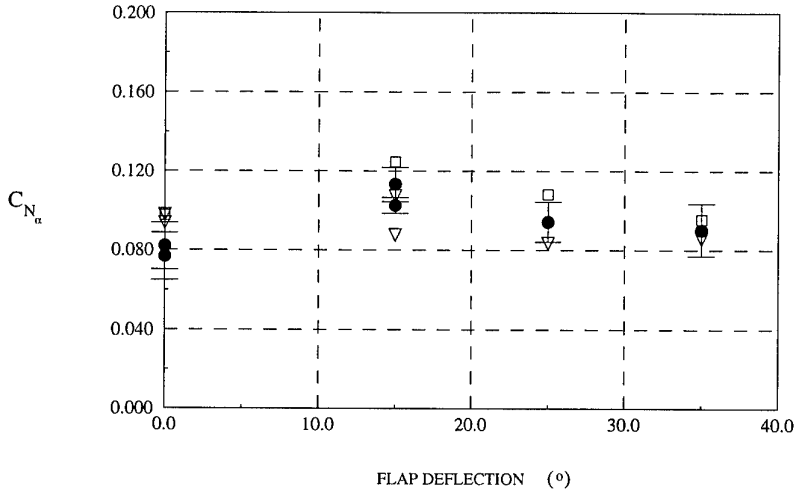

● flight test
▽ wind tunnel (flight cg)
□ wind tunnel (reference cg)

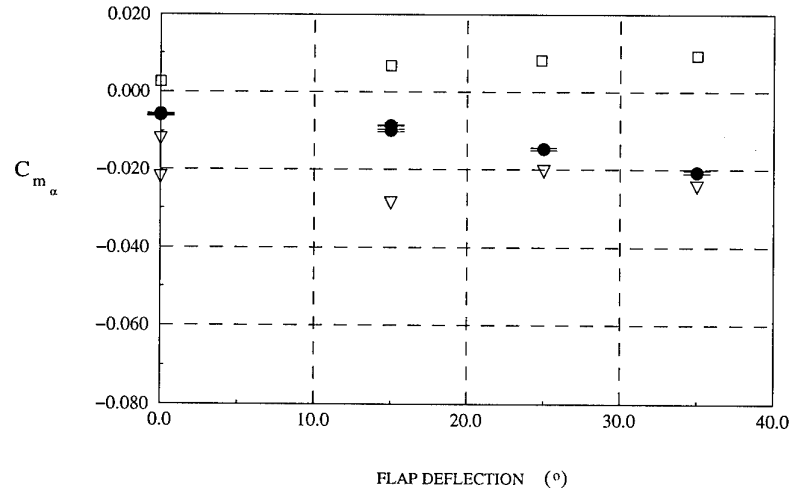

Figure 11: C_{N_α} and C_{m_α} derivatives as a function of flap deflection for $\Lambda = 16°$

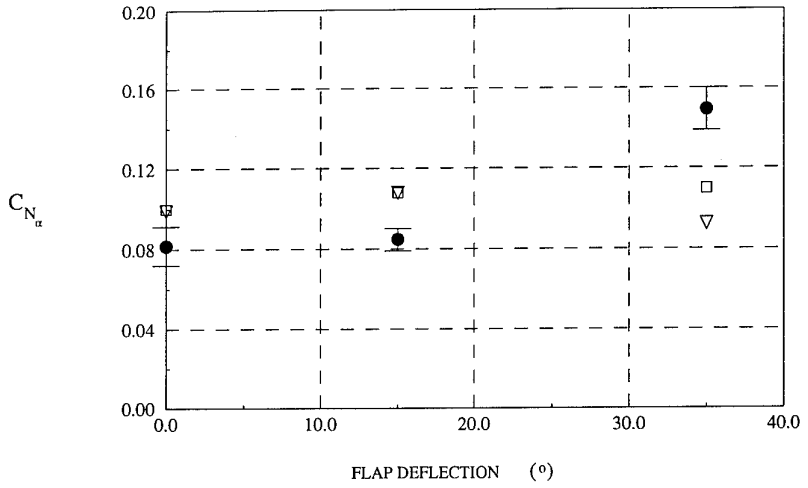

● flight test
▽ wind tunnel (flight cg)
□ wind tunnel (reference cg)

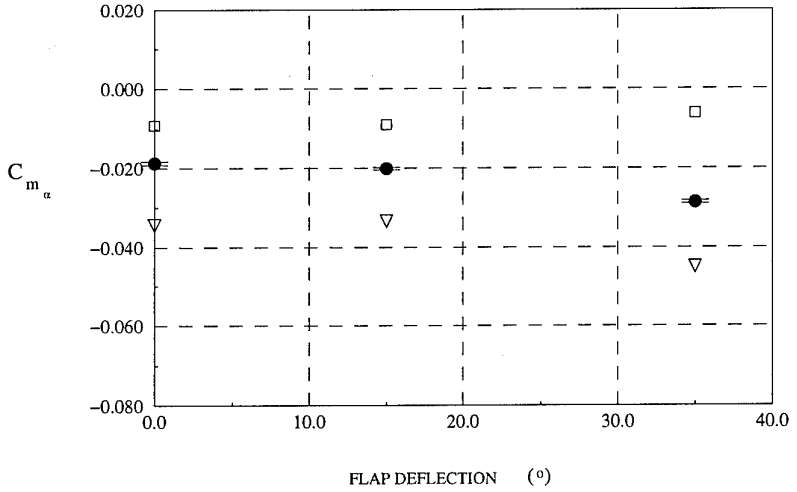

Figure 12: C_{N_α} and C_{m_α} derivatives as a function of flap deflection for $\Lambda = 26°$

pitch damping control system switched off would not be safe because of the resulting deterioration in the aircraft handling behaviour. As a result of the difficulties involved in obtaining an accurate estimate of the C_{m_q} derivative, the final estimates for both 16° and 26° wing sweep exhibited a greater degree of variability in their identification than the other longitudinal derivatives.

$C_{m_{\dot{\alpha}}}$ and C_{m_q} are difficult to identify separately. However it should be noted that some success has been met using the maximum likelihood technique with specially designed manoeuvres, such as two-point hesitation rolls [25]. In [15], [16] and [17], the $C_{m_{\dot{\alpha}}}$ and C_{m_q} derivatives were estimated using the MMLE3 'hard constraints' facility, i.e. the value of one derivative was constrained to be a multiple of the other. $C_{m_{\dot{\alpha}}}$ was estimated from C_{m_q} using this technique and the results matched the wind tunnel data well. In pEst however, there is no provision for such 'hard constraints', and so for the take-off and landing configuration cases it was decided to accept the wind tunnel $C_{m_{\dot{\alpha}}}$ values and identify only C_{m_q}. Earlier estimation carried out on the clean aircraft configuration [15], [16], [17], had shown sufficient agreement between the estimated $C_{m_{\dot{\alpha}}}$ values and the wind tunnel data to support this decision.

5.1.3 Control Derivatives

In a similar fashion to C_{m_q} and $C_{m_{\dot{\alpha}}}$, the derivatives C_{N_q} and $C_{N_{\delta_e}}$ were estimated for the clean configuration [15], [16], [17], using the MMLE3 'hard constraint' facility due to the difficulty in identifying them separately. Again, since there is no provision for 'hard constraints' in pEst, C_{N_q} was fixed using the wind tunnel values as a priori data. The measurement of dynamic derivatives in wind tunnels, for example C_{N_q}, is generally difficult in comparison to static derivatives, such as $C_{N_{\delta_e}}$, but as with $C_{m_{\dot{\alpha}}}$ there had been sufficient agreement between the estimated C_{N_q} values and the wind tunnel data for the clean configuration [15], [16], [17] to justify this decision.

For the 16° wing sweep case, the flight test results for $C_{N_{\delta_e}}$ and $C_{m_{\delta_e}}$ compare well with the wind tunnel data, although the Cramer-Rao bounds indicate a higher level of confidence in the $C_{m_{\delta_e}}$ estimates than the $C_{N_{\delta_e}}$ estimates. At 26° wing sweep the flight test results for $C_{m_{\delta_e}}$ also compare well with the wind tunnel data, differing by less than 15%.

5.2 Lateral Derivatives

The output-error parameter estimation program, pEst, was applied to each lateral manoeuvre. For wing sweeps less than 47° spoilers are automatically deployed for roll control in addition to the aileron deflection [4]. Hence in all take-off and landing configurations, where the wing sweep is always less than 47°, both spoilers and ailerons are used as inputs. The following measurands were used as responses :

- angle-of-sideslip, β,
- roll rate, p,
- yaw rate, r,

	Side Force	Rolling Moment	Yawing Moment
Aerodynamic	C_{Y_β}	C_{l_β} C_{l_p}	C_{n_β} C_{n_r}
Control	$C_{Y_{\delta_r}}$	$C_{l_{\delta_r}}$ $C_{l_{\delta_{sp}}}$ $C_{l_{\delta_a}}$	$C_{n_{\delta_r}}$ $C_{n_{\delta_{sp}}}$

Table 7: Lateral derivatives estimated

- lateral acceleration, a_y, and
- roll attitude, ϕ.

The roll attitude (ϕ) was recorded but was initially given zero weighting in the identification process for the clean aircraft configuration [20], [21], [22]. However, acceptable time history matches were difficult to obtain in the take-off and landing configuration without ϕ matching. The match improved considerably when ϕ was included as an output match.

An example of the time histories for these output variables for a given rudder and aileron input is shown in figure 13. The time history plots shown in figure 13 and the Cramer-Rao bounds were used to assess the accuracy of the identification procedure.

The lateral derivatives identified are given in table 7 and the results shown in figures 14, 15, 16 and 17.

5.2.1 Angle-of-Sideslip Derivatives

The static lateral aerodynamic derivatives are the side force, rolling and yawing moments due to sideslip, C_{Y_β}, C_{l_β} and C_{n_β} respectively. For the side force due to sideslip derivative C_{Y_β}, the flight test results show little scatter and agree well with the wind tunnel results.

The derivative C_{l_β}, known as the dihedral effect, matches the wind tunnel data well for 16° wing sweep. At 26° wing sweep the magnitudes of the flight data are consistently less than that of the wind tunnel values by approximately 30%. The C_{l_β} estimates displayed similar behaviour in [20], [21] and [22] for the clean aircraft configuration.

The weathercock stability derivative, C_{n_β}, results shows little scatter at most flight conditions. For 16° wing sweep the flight test data tends to be about 40% of the wind tunnel value. At 26° wing sweep the flight data tends to be about 50% of the wind tunnel value. This is consistent with the results given in [20], [21] and [22] where the wind tunnel results regularly overestimated values of C_{n_β}.

5.2.2 Roll and Yaw Rate Derivatives

The aerodynamic derivatives with the largest identification variability are the side force due to roll and yaw rate derivatives, C_{Y_p} and C_{Y_r}, the rolling moment due to yaw rate derivative C_{l_r},

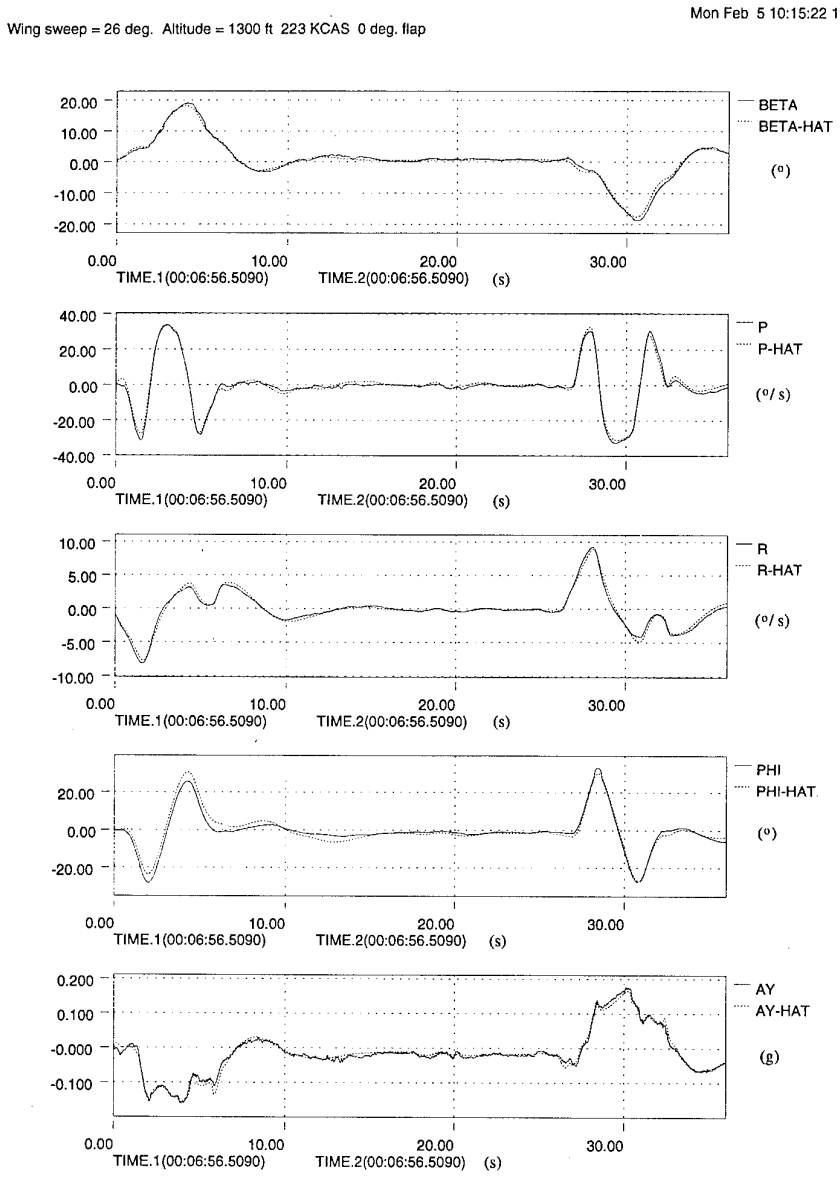

Figure 13: Lateral response to aileron and rudder doublet for case p1f6e38c

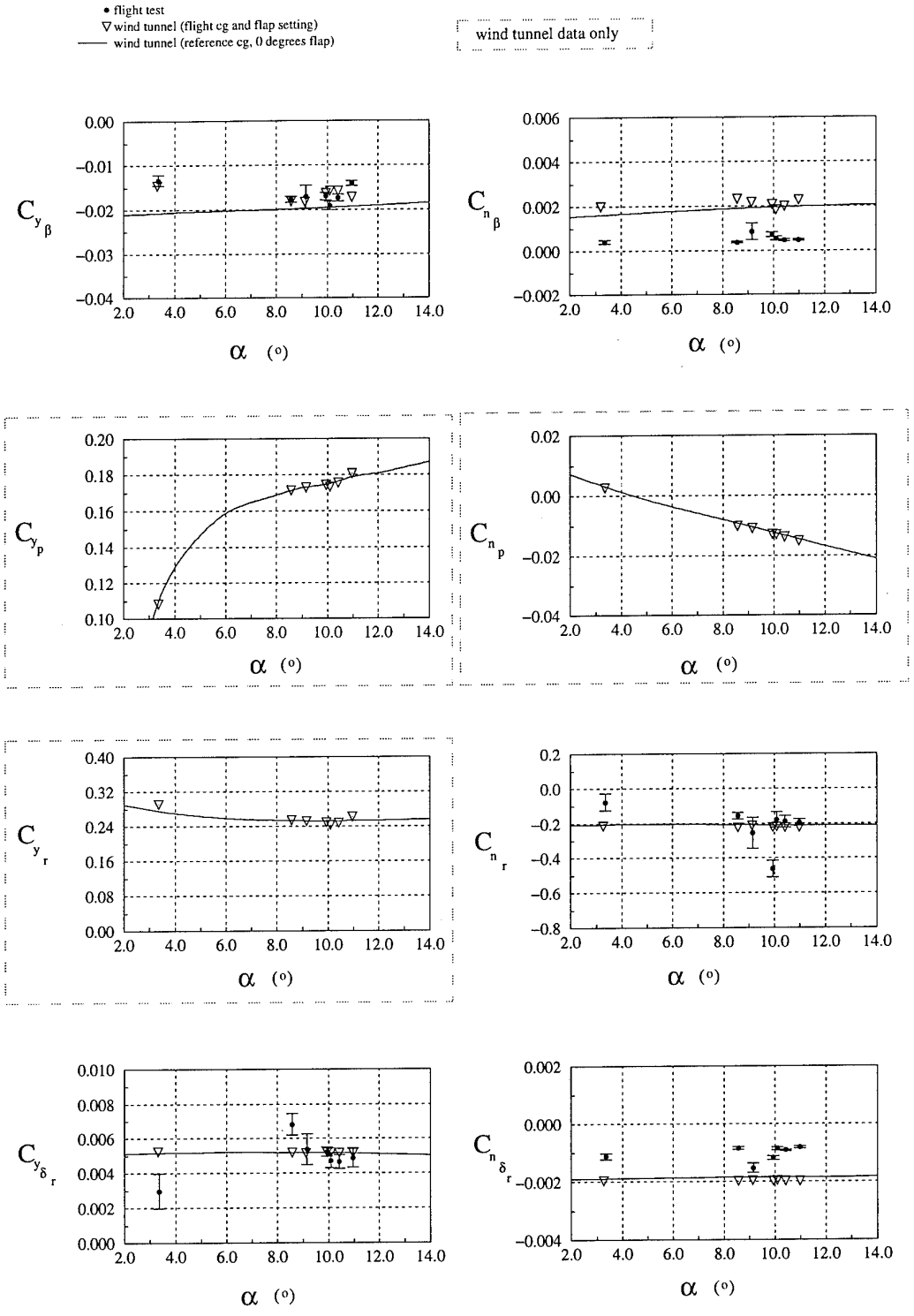

Figure 14: Lateral aerodynamic derivatives for $\Lambda = 16°$

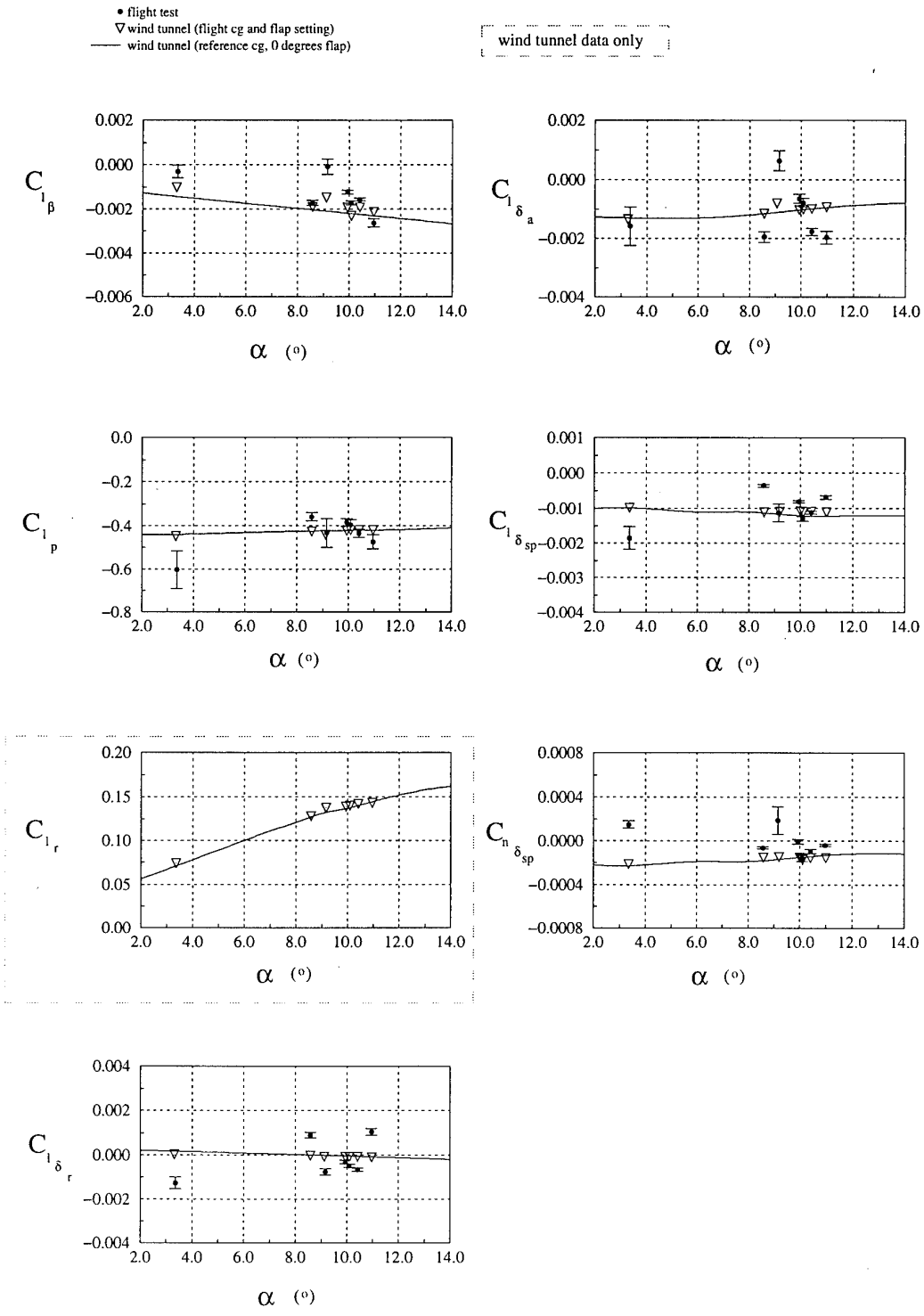

Figure 15: Lateral aerodynamic derivatives for $\Lambda = 16°$ (continued)

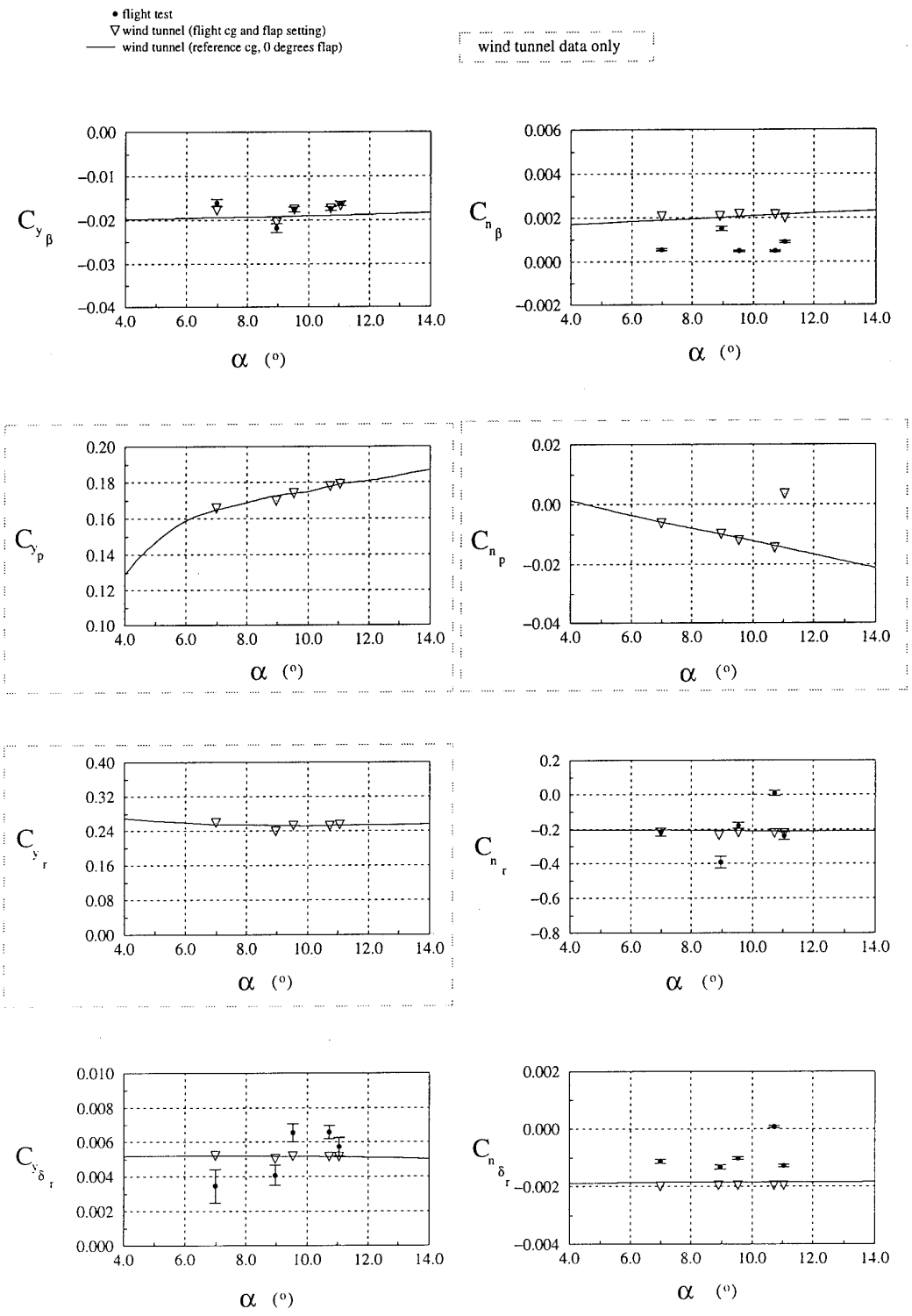

Figure 16: Lateral aerodynamic derivatives for $\Lambda = 26°$

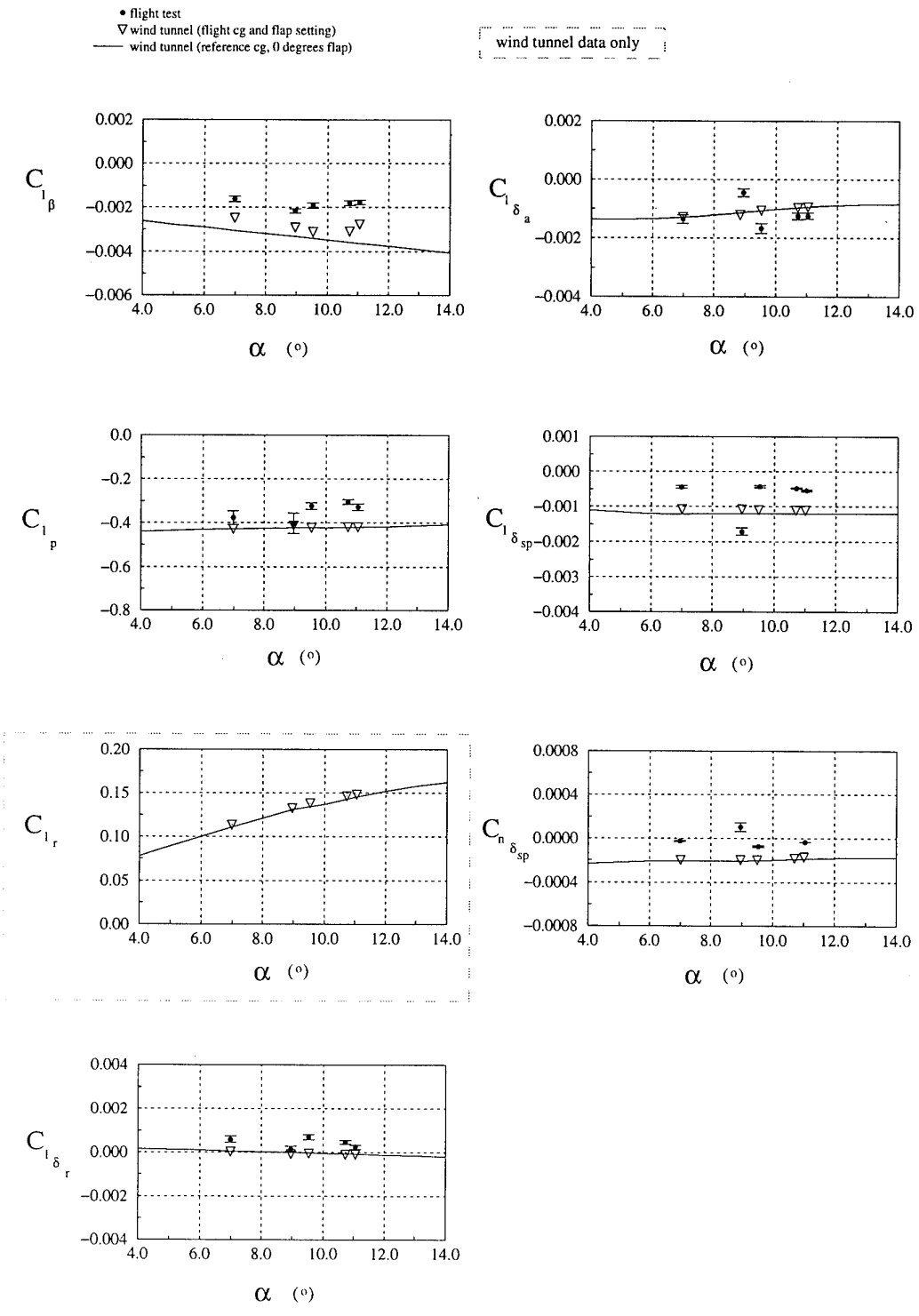

Figure 17: Lateral aerodynamic derivatives for $\Lambda = 26°$ (continued)

and the yawing moment due to roll rate derivative C_{n_p}. In general for conventional aircraft such as the F-111C, C_{Y_p} and C_{Y_r} are not physically significant, whereas the cross derivatives C_{l_r} and C_{n_p} may be significant but the responses from the lateral manoeuvres contain little information to determine these derivatives. Therefore they were not estimated but were fixed at the a priori values.

Although the match obtained using the a priori data was quite acceptable, some of the identified parameters were obviously incorrect. For example, the estimated value of the non-dimensional yawing moment due to yaw rate derivative C_{n_r}, which is a damping term, was positive where a negative value was expected. It was found that $C_{n_{\dot{\beta}}}$ and C_{n_r} were linked; if one was fixed while the other was identified, the sum of the two effects was the same as if both were being identified. Hence the $\dot{\beta}$ terms were fixed at zero and their contribution was accounted for by identifying the yaw rate derivatives, i.e. C_{Y_r}, C_{l_r} and C_{n_r}. The match was still good, and C_{n_r} had the correct sign for all cases and reasonable magnitudes, although it does exhibit a large degree of scatter about the wind tunnel data points. This is partly a result of the aircraft control system being engaged during the flight test programme. The large rapid control inputs, necessary for the identification process, are quickly damped by the control system, resulting in reduced identification accuracy of the yaw damping derivative, C_{n_r}.

For the 16° wing sweep case the flight test results agree well with the wind tunnel data. These trends are reinforced by similar trends for the clean configuration in [20], [21] and [22]. Results for the roll damping derivative C_{l_p}, while of the correct sign, are approximately 25% lower in magnitude than the wind tunnel results for the 26° wing sweep case, but display similar trends.

5.2.3 Control Derivatives

The lateral control derivatives consist of side force, rolling and yawing moments due to aileron, rudder and spoiler deflections, $C_{Y_{\delta_a}}$, $C_{Y_{\delta_r}}$, $C_{Y_{\delta_{sp}}}$, $C_{l_{\delta_a}}$, $C_{l_{\delta_r}}$, $C_{l_{\delta_{sp}}}$, $C_{n_{\delta_a}}$, $C_{n_{\delta_r}}$ and $C_{n_{\delta_{sp}}}$.

For wing sweeps of less than 47°, roll control activates both aileron and spoiler. The moments produced by these controls are similar and so their individual contributions are difficult to separate. Neither spoilers nor ailerons contribute significantly to the total side force, and ailerons cause little yawing moment. Accordingly, the derivatives $C_{Y_{\delta_a}}$, $C_{Y_{\delta_{sp}}}$ and $C_{n_{\delta_a}}$ are of minor importance. In order to improve the identification process they were therefore fixed at their a priori values and only $C_{Y_{\delta_r}}$, $C_{l_{\delta_a}}$, $C_{l_{\delta_r}}$, $C_{l_{\delta_{sp}}}$, $C_{n_{\delta_r}}$ and $C_{n_{\delta_{sp}}}$ were identified.

The non-dimensional sideforce due to rudder deflection derivative, $C_{Y_{\delta_r}}$ is small in magnitude and of secondary importance. The flight test results, in general, agree well with the wind tunnel data for 16° wing sweep. At 26° wing sweep, the flight test results display considerably more scatter about the wind tunnel data. The non-dimensional rolling moment due to rudder deflection derivative, $C_{l_{\delta_r}}$ is also small in magnitude and of secondary importance. The flight test results are scattered about the wind tunnel data at 16° wing sweep. At 26° wing sweep the flight test results agree well with the wind tunnel data.

The non-dimensional rolling moment due to aileron deflection derivative, $C_{l_{\delta_a}}$ shows considerable scatter for 16° wing sweep but at 26° wing sweep the flight test results agree well with the wind tunnel data.

The non-dimensional rolling moment due to spoiler deflection derivative, $C_{l_{\delta_{sp}}}$ is a primary roll

control derivative. For 16° wing sweep the flight test results show good agreement with the wind tunnel data. At 26° wing sweep the results are consistently lower in magnitude than the wind tunnel data by approximately 50%, with the exception of a single point at an angle-of-attack of 9°.

The non-dimensional yawing moment due to rudder deflection derivative, $C_{n_{\delta_r}}$ is a primary lateral control derivative. For both wing sweep angles the flight test results are lower in magnitude than the wind tunnel data by as much as 50%. This is similar to the clean aircraft case, [20], [21], [22], where the estimation procedure consistently estimated $C_{n_{\delta_r}}$ to be approximately 65% lower in magnitude than the wind tunnel data whilst still following the same trends.

The non-dimensional yawing moment due to spoiler deflection derivative, $C_{n_{\delta_{sp}}}$ is a small, secondary lateral control derivative and the flight test results in general show reasonable agreement with the wind tunnel data. At 26° wing sweep the results are consistently lower in magnitude than the wind tunnel data by approximately 50%.

It should be noted that for both the 16° and 26° wing sweep cases there are flight test points that show a positive $C_{n_{\delta_{sp}}}$. Positive spoiler deflection corresponds to the port spoiler deflected upwards, as is shown in figure 1, and the increased drag produced by the port wing would result in a negative yawing moment. Therefore the derivative $C_{n_{\delta_{sp}}}$ is expected to be negative. However, at low Mach number and moderate wing sweep the derivative $C_{n_{\delta_{sp}}}$ is reduced and any errors introduced into the estimation of $C_{n_{\delta_{sp}}}$ become significant, the noticeably larger Cramer-Rao bounds on the points in question indicate the reduced degree of confidence in these results. The reversed sign of some of the $C_{n_{\delta_{sp}}}$ points is indicative of the difficulty involved in obtaining the F-111C spoiler derivatives. Reference [27] details additional research being carried out into spoiler characteristics.

5.3 Summary

The flight-estimated aerodynamic derivatives are generally in agreement with the wind tunnel values. There are three exceptions; the pitch stiffness, C_{m_α}, the yaw stiffness, C_{n_β} and the yawing moment due to rudder derivative, $C_{n_{\delta_r}}$. The flight estimates are consistently less than the wind tunnel derivatives and this result was also found for the clean aircraft configuration, [15], [16], [17], [20], [21] and [22]. NASA Dryden reports also agree with this trend [26]. The wind tunnel results for the yawing moment derivatives of the F-111C are not unlike those of other aircraft test programs carried out in the 1960's. These derivatives are susceptible to model sting-support interference. However, no details of the wind tunnel facility, model size and accuracy or the test procedure are available to confirm this.

The augmented pitch and yaw damping provided by the automatic flight control system, whilst modifying the aircraft's natural response, also reduces the identifiability of a number of secondary derivatives. This also appears to have contributed to the reduction in the values of the pitch and yaw stiffness derivatives identified.

The results also indicate that for the 26° wing sweep case there is a tendency to underestimate the spoiler derivatives, $C_{l_{\delta_{sp}}}$ and $C_{n_{\delta_{sp}}}$ as well as the dihedral effect, C_{l_β}. The clean aircraft configuration does not show this trend. There is no obvious reason for this behaviour and the NASA results published do not cover the take-off and landing configurations.

Decoupling the spoiler and differential stabilator, i.e. aileron, derivatives resulted in identification difficulties. Combining the spoiler and aileron effects [26], whilst improving identifiability, does not allow simple comparison with wind tunnel data.

6 CONCLUSIONS

Stability and control derivatives describing the longitudinal and lateral aerodynamic characteristics of the F-111C have been determined from flight test measurements. The results presented in this report are for 16° and 26° wing sweep angles with the aircraft in the take-off and landing configurations. Details of the flight test schedule and the data processing and analysis procedures have been presented.

The flight test program covered only limited take-off and landing test points thus only limited validation over the wider angle-of-attack range of the wind tunnel data was possible. In general all primary longitudinal and lateral derivatives show satisfactory repeatability and indicated similar trends to the wind tunnel data.

Estimates for the C_{m_α}, C_{n_β} and $C_{n_{\delta_r}}$ derivatives were consistently lower in magnitude than the corresponding wind tunnel data. This is consistent with the clean aircraft results given in [15], [16], [17], [20], [21] and [22]. For the 26° wing sweep cases, the two spoiler derivatives $C_{l_{\delta_{sp}}}$ and $C_{n_{\delta_{sp}}}$, and C_{l_β} were underestimated. Further research is underway into obtaining more accurate estimates of spoiler characteristics [27].

ACKNOWLEDGEMENTS

The authors wish to acknowledge the support received from Geoff Brian, Mark Cooper, Colin Martin and Peter Gibbens at AMRL.

REFERENCES

[1] 'Final Preliminary Stability and Control Aerodynamic Data for the F-111B Airplane', FZM-12-4207, General Dynamics, Fort Worth Division, Fort Worth, TX, USA, 23 November 1966.

[2] 'Final Preliminary Stability and Control Aerodynamic Data for the F-111A Airplane', FZM-12-4198, General Dynamics, Fort Worth Division, Fort Worth, TX, USA, 1 October 1965.

[3] 'Final Flight Control Subsystem Engineering Report for the F-111A Aircraft', FZM-12-13468, General Dynamics, Fort Worth Division, Fort Worth, TX, USA, 18 May 1973.

[4] Cooper, M. I., 'A Flight Dynamics Model of the F-111C Using the Simulation Language ACSL', ARL Aerodynamics Report 166, Melbourne, Victoria, Australia, December 1985. (Confidential)

[5] Cooper, M. I., Drobik, J. S. and Martin, C. A., 'F-111C Flight Data Reduction and Analysis Procedures', Flight Mechanics Report 187, DSTO Aeronautical Research Laboratory, Melbourne, Victoria, Australia, December 1990.

[6] Rundle, T. D., 'Validation of the F-111C Flight Dynamics Mathematical Model', ARDU-TS-1691, RAAF Aircraft Research and Development Unit, Salisbury, SA, Australia, August 1988. (Restricted)

[7] Special Document AEL-0269-SD, 'Nose Boom Transducing Unit (NBTU), Installation, Operation and Maintenance Manual', Advanced Engineering Laboratory, Salisbury, SA, Australia, June 1988.

[8] 'ARDU AFTRAS Data User's Manual', RAAF Aircraft Research and Development Unit, Edinburgh, SA, Australia, 6 March 1985.

[9] Blackwell, J., 'A Maximum Likelihood Parameter Estimation Program for General Non-Linear Systems', ARL Aerodynamics Technical Memorandum 392, Melbourne, Victoria, Australia, January 1988.

[10] Martin, C. A. and Cooper, M. I., 'A Method for the In-Flight Calibration of Sideslip and Angle-of-Attack Flow Direction Vanes', ARL ABS-FW Group Report 86/4, Melbourne, Victoria, Australia, June 1986.

[11] Norton, J. P., De Souza, C. E., Evans, R. J. and Goodwin, G. C, 'Nonlinear Estimation Algorithms for Aircraft Flight Path Reconstruction', Technical Report EE8340, Department of Electrical and Computer Engineering, University of Newcastle, NSW, Australia, October 1983.

[12] De Souza, C. E. and Goodwin, G. C., 'User's Guide for the Flight Path Reconstruction Programmes', Annex to Technical Report EE8340, Department of Electrical and Computer Engineering, University of Newcastle, NSW, Australia, June 1986.

[13] Maine, R. E. and Iliff, K. W., 'Application of Parameter Estimation to Aircraft Stability and Control: *The Output-Error Approach*', NASA Reference Publication 1168, Dryden Flight Research Facility, NASA Ames Research Center, Edwards, CA, USA, June 1986.

[14] Murray, J. E. and Maine, R. E., 'pEst Version 2.1 User's Manual', NASA Technical Memorandum 88280, Dryden Flight Research Facility, NASA Ames Research Center, Edwards, CA, USA, September 1987.

[15] MacLaren, L. D., Martin, C. A., Cooper, M. I. and Drobik, J. S., 'F-111C Longitudinal Aerodynamic Flight Data Analysis for Wing Sweeps 16° and 26°', Flight Mechanics Report 181, DSTO Aeronautical Research Laboratory, Melbourne, Victoria, Australia, December 1990. (Restricted)

[16] MacLaren, L. D., Martin, C. A., Cooper, M. I. and Drobik, J. S., 'F-111C Longitudinal Aerodynamic Flight Data Analysis for Wing Sweeps 35° and 45°', Flight Mechanics Report 182, DSTO Aeronautical Research Laboratory, Melbourne, Victoria, Australia, January 1991. (Restricted)

[17] Cooper, M. I., Martin, C. A., Drobik, J. S. and Gibbens, P. W., 'F-111C Longitudinal Aerodynamic Flight Data Analysis for Wing Sweeps 50° and 72.5°', Flight Mechanics Report 183, DSTO Aeronautical Research Laboratory, Melbourne, Victoria, Australia, January 1991. (Restricted)

[18] Maine, R. E. and Iliff, K. W., 'User's Manual for MMLE3, a General FORTRAN Program for Maximum Likelihood Parameter Estimation', NASA Technical Paper 1563, Dryden Flight Research Center, Edwards, CA, USA, 1980.

[19] Maine, R. E. and Iliff, K. W., 'The Theory and Practice of Estimating the Accuracy of Dynamic Flight-Determined Coefficients', NASA Reference Publication 1077, Dryden Flight Research Center, Edwards, CA, USA, 1981.

[20] Drobik, J. S., Martin, C. A. and Cooper, M. I. 'F-111C Lateral Aerodynamic Flight Data Analysis for Wing Sweeps 16° and 26°', Flight Mechanics Report 184, DSTO Aeronautical Research Laboratory, Melbourne, Victoria, Australia, February 1992. (Restricted)

[21] Drobik, J. S., Martin, C. A. and Cooper, M. I. 'F-111C Lateral Aerodynamic Flight Data Analysis for Wing Sweeps 35° and 45°', Flight Mechanics Report 185, DSTO Aeronautical Research Laboratory, Melbourne, Victoria, Australia, December 1991. (Restricted)

[22] Drobik, J. S., Martin, C. A., Cooper, M. I. and Gibbens, P. W., 'F-111C Lateral Aerodynamic Flight Data Analysis for Wing Sweeps 50° and 72.5°', Flight Mechanics Report 186, DSTO Aeronautical Research Laboratory, Melbourne, Victoria, Australia, December 1990. (Restricted)

[23] Brian, G. J., 'F-111C Flight Dynamic Model Aerodynamic Database Development', DSTO Technical Report (In preparation), Melbourne, Victoria, Australia.

[24] Etkin, B., 'Dynamics of Atmospheric Flight', John Wiley & Sons Inc., New York, NY, USA, 1972.

[25] Maine, R. E. and Iliff, K. W., 'Maximum Likelihood Estimation of Translational Acceleration Derivatives from Flight Data', Journal of Aircraft, vol. 16, no. 10, October 1979, pp. 674-679.

[26] Iliff, K. W., Maine, R. E. and Steers, S. T., 'Flight-Determined Stability and Control Coefficients of the F-111A Airplane', NASA Technical Memorandum 72851, NASA Dryden Flight Research Facility, Edwards, CA, USA, March 1978.

[27] Stuckey, R. A., 'Flight-Estimated Spoiler Aerodynamics of the F-111C Aircraft', AIAA Atmospheric Flight Mechanics Conference, Scottsdale, AZ, USA, Paper 94-3459, August 1994, pp. 449-458.

[28] De Souza,C. E., Evans,R. J. and Goodwin,G. C., 'Nonlinear Estimation Algorithms for Flight Path Reconstruction', University of Newcastle, Department of Electrical and Computer Engineering, Technical Report EE8316, Newcastle, NSW, Australia, March 1983.

APPENDIX A
CALIBRATION OF ANGLE-OF-ATTACK SENSORS

The angle-of-attack sensor position errors for the CADS used in Phase 1, and NBTU used in Phase 3, were calculated using a flight path reconstruction computer program [28]. The program uses measured values of longitudinal and normal acceleration and pitch rate as inputs to a set of equations describing the longitudinal kinematic relationships. From the state variables, the body axes velocities (u and w) and pitch attitude (θ), the output quantities angle-of-attack and altitude (α and H) are calculated. The flight path reconstruction technique uses an extended Kalman filter to determine the calibration parameters relating the computed and measured output variables. For the angle-of-attack instrument, the calibration is assumed to be linear with a slope K_α and bias b_α. The bias term is not needed in the parameter estimation stage since bias errors are accounted for separately.

The flight path reconstruction software assumes that the measured angle of attack may be described by an equation of the form :

$$\alpha_m = (1 + \lambda_\alpha)\alpha_{true} + b_\alpha \tag{A1}$$

where λ_α and b_α are the scale factor and bias respectively and the subscripts m and t indicate the measured and true values respectively. In the flight path reconstruction software, terms which adjust the α measurement to the cg position are accounted for, as are the effects of the vane sensor displacement from the cg, by making use of the instrument locations with respect to the cg.

The aerodynamic estimation software, pEst [14], defines an upwash factor, or flow amplification, for the angle-of-attack sensor, K_α, such that :

$$\alpha_{\tilde{z}} = K_\alpha[\alpha_{true}] - (x_\alpha - x_{cg})\frac{q}{V} + (y_\alpha - y_{cg})\frac{p}{V} + \alpha_b \tag{A2}$$

where α_z is the computed response or the equivalent of the true α.

The upwash factor in pEst can be expressed in a similar form to that of equation A1 :

$$K_\alpha = (1 + \lambda_\alpha) \tag{A3}$$

The variation of K_α versus true airspeed is given in figure A1 for both Phase 1 and 3 cases. While there is some variation in K_α with Mach number and wing sweep angle, these variations are not significant within the accuracy of the data and so a constant value of 1.04 was chosen for Phase 1 compared with 0.94 for the cruise configuration. An investigation into the effect of K_α variation showed that errors in K_α of 10 % resulted in an adjustment of typically 5 % in the major derivatives. The difference between the clean and take-off and landing configuration results is postulated to be a consequence of the upstream influence of the aerodynamically 'dirty' take-off and landing configuration.

Only three Phase 3 cases were available. Hence the K_α value calculated for each case was used. K_α values of approximately 1.17 were calculated for the Phase 3 take-off and landing configuration cases compared with a value of 1.06 for the clean configuration.

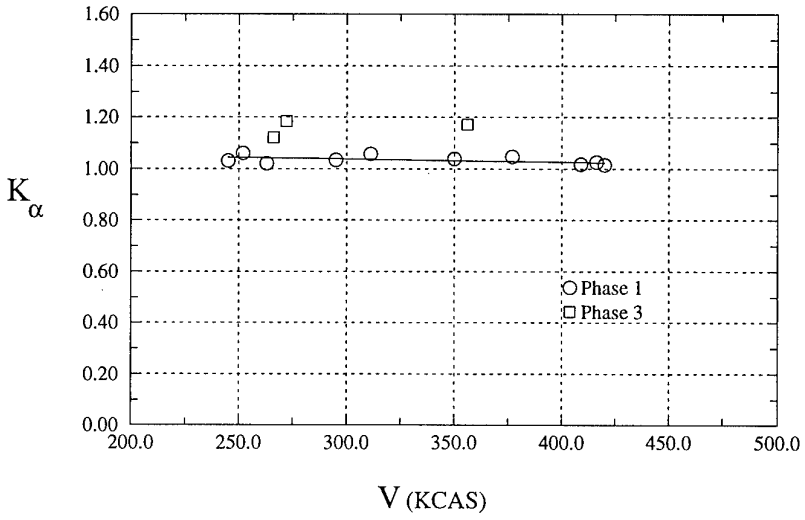

Figure A1: Angle-of-attack scale factor

APPENDIX B
CALIBRATION OF ANGLE-OF-SIDESLIP SENSOR

The angle-of-sideslip sensor position errors for the CADS used in Phase 1, and NBTU used in Phase 3, were calculated using the full six degree-of-freedom mode of the flight path reconstruction computer program [28]. The program uses measured values of longitudinal, lateral and normal accelerations and pitch, roll and yaw rates as inputs to a set of equations describing the full six degree-of-freedom kinematic relationships. From the state variables, the body axes velocities (u, v and w) and roll, pitch and yaw attitudes (ϕ, θ and ψ), the output quantities of velocity, angle-of-attack, angle-of-sideslip, bank and pitch angle and altitude ($V, \alpha, \beta, \phi, \theta$ and H) are calculated. The flight path reconstruction technique uses an extended Kalman filter to determine the calibration parameters relating the computed and measured output variables. For the angle-of-sideslip instrument, the calibration is assumed to be linear with a slope K_β and bias b_β. The bias term is not needed in the parameter estimation stage since bias errors are accounted for separately.

The flight path reconstruction software assumes that the measured angle of sideslip may be described by an equation of the form :

$$\beta_m = (1 + \lambda_\beta)\beta_{true} + b_\beta \tag{B1}$$

where λ_β and b_β are the scale factor and bias respectively and the subscripts m and t indicate the measured and true values respectively. In the flight path reconstruction software, terms which adjust the β measurement to the cg position are accounted for, as are the effects of the vane sensor displacement from the cg, by making use of the instrument locations with respect to the cg.

The aerodynamic estimation software, pEst [14], defines a sidewash factor, or flow amplification, for the angle-of-sideslip sensor, K_β, such that :

$$\beta_{\tilde{z}} = K_\beta[\beta_{true}] + (z_\beta - z_{cg})\frac{p}{V} - (x_\beta - x_{cg})\frac{r}{V} + \beta_b \tag{B2}$$

where β_z is the computed response or the equivalent of the true β.

The sidewash factor in pEst can be expressed in a similar form to that of equation B1 :

$$K_\beta = (1 + \lambda_\beta) \tag{B3}$$

The variation of K_β with true airspeed is given in figure B2 for both Phase 1 and Phase 3 cases. The CADS angle-of-sideslip sensor overestimated the true value by approximately 55% for Phase 1 take-off and landing configuration cases. The clean aircraft configuration results indicated that K_β was overestimated by approximately 60%. As with the angle-of-attack sensor only three cases were available from the Phase 3 flights hence the individual K_β values were used in the analysis. The NBTU, as expected, gave closer estimates of the true angle-of-sideslip, varying by only $\pm 10\%$. This result is similar to that obtained for the clean configuration case.

An investigation into the affect of K_β variation showed that, in general, changes in K_β of 10 % resulted in maximum changes of 5 % in the derivatives.

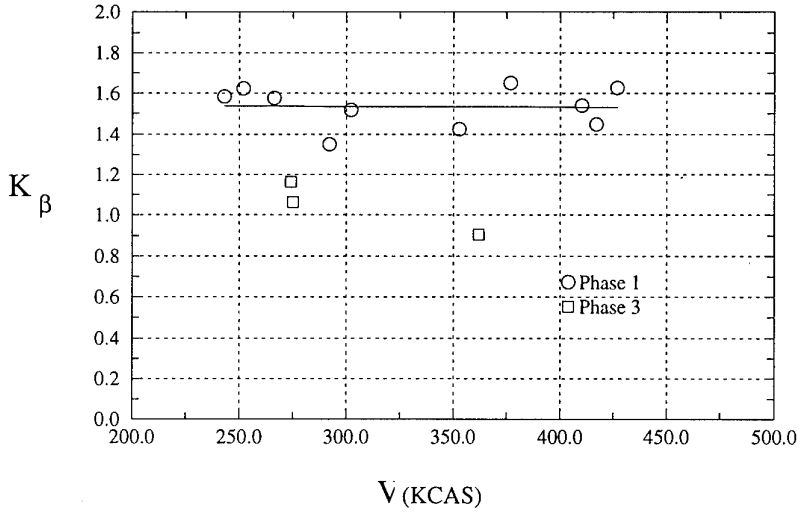

Figure B2: Angle-of-sideslip scale factor

APPENDIX C - SAMPLE LONGITUDINAL pEst OUTPUT

pEst: *Slanted text* represents user inputs. Units are defined in pEst manual [14].

pEst program for parameter estimation
Richard Maine/James Murray - NASA Dryden
version 2.3.4 10 Aug 90
this run date: time:

Help is available

pEst: *read m.p1f6e01c*

reading measured time history from file "m.p1f6e01c"
signal d1 not found. Using 0.
signal d2 not found. Using 0.
signal d4 not found. Using 0.
signal thrust not found. Using 0.

pEst: *restore c.p1f6e01c.final*

reading program status from file "c.p1f6e01c.final"

checking consistency of file "c.p1f6e01c.final" and file "m.p1f6e01c"

pEst: *states*
name on? limit name on? limit name on? limit

alpha T .1000E+05 q T .1000E+05 theta T .1000E+05

pEst: *resp*
name weight on? name weight on?

alpha 27.00 T theta 13.00 T
q 13.00 T an 200.0 T

pEst: *sho stats*

signal	average	signal	average	signal	average
de	-1.58	q	-.145E-02	ay	-.198E-01
d1	.000E+00	theta	4.21	pdot	-.824
d2	.000E+00	an	1.00	rdot	-1.02
da	.845E-01	ax	-.883E-01	qbar	193.
dr	-.425	qdot	1.14	mach	.363
d3	-.224	beta	.339	thrust	.000E+00
d4	.000E+00	p	-.386	alt	353.
v	405.	r	-.650E-01		
alpha	5.97	phi	-1.08		

pEst: *do mmle3.para.p1f6e01c*
reading from command file.

pEst: *par xa -25.4766*
name value on?

xa -25.48 F

pEst: *par ya 0.0000*
name value on?

ya .0000E+00 F

pEst: *par za -1.5204*
name value on?

za -1.520 F

pEst: *par xb -32.1599*
name value on?

xb -32.16 F

pEst: *par yb 0.0000*
name value on?

yb .0000E+00 F

pEst: *par zb -3.5121*
name value on?

zb -3.512 F

pEst: *par xax -2.5416*
name value on?

xax -2.542 F

pEst: *par yax -2.4308*
name value on?

yax -2.431 F

pEst: *par zax -1.4371*
name value on?

zax -1.437 F

pEst: *par xay -2.4391*
name value on?

xay -2.439 F

pEst: *par yay -2.4583*
name value on?

yay -2.458 F

pEst: *par zay -1.4371*
name value on?

zay -1.437 F

pEst: *par xan -2.5416*
name value on?

xan -2.542 F

pEst: *par yan -2.3617*
name value on?

yan -2.362 F

pEst: *par zan -1.4371*
name value on?

zan -1.437 F

pEst: *const ix 73674.3359*
name value

ix .7367E+05

pEst: *const iy 387397.3750*
name value

iy .3874E+06

pEst: *const iz 453923.0313*
name value

iz .4539E+06

pEst: *const ixz 2542.6226*
name value

ixz 2543.

pEst: *const mass 2334.9495*
name value

mass 2335.

pEst: *const xcg 0.0*
name value

xcg .0000E+00

pEst: *const ycg 0.0*
name value

ycg .0000E+00

pEst: *const zcg 0.0*
name value

zcg .0000E+00

pEst: *resp alpha w=18*
name weight on?

alpha 18.00 T

pEst: *resp q w=13*
name weight on?

q 13.00 T

pEst: *resp theta w=13*
name weight on?

theta 13.00 T

pEst: *resp an w=200*
name weight on?

an 200.0 T

pEst: *par cnorm0*
name value on?

cNorm0 .1767 T

pEst: *par cnorma*
name value on?

cNorma .1025 T

pEst: *par cnormde*
name value on?

cNormde .1543E-01 T

pEst: *par cma*
name value on?

cma -.8652E-02 T

pEst: *par cmq*
name value on?

cmq -35.36 T

pEst:
command file done.

pEst: *it 20*

name	value	on?	name	value	on?	name	value	on?
cNorm0	.1767	T	cNormde	.1543E-01	T	cmq	-35.36	T
cNorma	.1025	T	cma	-.8652E-02	T	cmde	-.3059E-01	T

total cost = 59.15
cost per response :

alpha	q	theta	an
56.9	38.4	29.2	112.

Iteration 1
Lev-Marq used 1 trials. v = .0000E+00 len = .3121E-01 cost = 59.15

name	value	on?	delta	name	value	on?	delta
cNorm0	.1767	T	.6425E-04	cma	-.8652E-02	T	-.3889E-06
cNorma	.1025	T	-.6514E-05	cmq	-35.36	T	.7772E-02
cNormde	.1543E-01	T	-.2783E-06	cmde	-.3059E-01	T	.1442E-06

total cost = 59.15
cost per response :

alpha	q	theta	an
56.9	38.4	29.2	112.

iteration 1 used 10 integrations
** iteration converged
estimate used 10 integrations

pEst: *par all*

name	value	on?	name	value	on?	name	value	on?
cNorm0	.1767	T	cmd2	.0000E+00	F	qBias	.0000E+00	F
cNorma	.1025	T	cmd3	.0000E+00	F	thetaBias	.0000E+00	F
cNorma2	.0000E+00	F	ca0	.0000E+00	F	anBias	.0000E+00	F
cNormAdot	2.544	F	caa	.0000E+00	F	axBias	.0000E+00	F
cNormq	5.806	F	caa2	.0000E+00	F	qdotBias	.0000E+00	F
cNormde	.1543E-01	T	caAdot	.0000E+00	F	ka	1.040	F
cNormde2	.0000E+00	F	caq	.0000E+00	F	xa	-25.48	F
cNormd1	.0000E+00	F	cade	.0000E+00	F	ya	.0000E+00	F
cNormd2	.0000E+00	F	cade2	.0000E+00	F	za	-1.520	F
cNormd3	.0000E+00	F	cad1	.0000E+00	F	xan	-2.542	F
cm0	.0000E+00	F	cad2	.0000E+00	F	yan	-2.362	F
cma	-.8652E-02	T	cad3	.0000E+00	F	zan	-1.437	F
cma2	.0000E+00	F	v0	.0000E+00	F	xax	-2.542	F
cmAdot	-4.665	F	alpha0	.0000E+00	F	yax	-2.431	F
cmq	-35.36	T	q0	.0000E+00	F	zax	-1.437	F
cmde	-.3059E-01	T	theta0	.0000E+00	F	xv	.0000E+00	F
cmde2	.0000E+00	F	vBias	.0000E+00	F	yv	.0000E+00	F
cmd1	.0000E+00	F	alphaBias	.0000E+00	F	zv	.0000E+00	F

name	value	on?	name	value	on?	name	value	on?
cy0	.7402E-01	F	cld3	-.1600E-02	F	rBias	.0000E+00	F
cyb	-.1230E-01	F	cld4	.0000E+00	F	phiBias	.0000E+00	F
cyb3	.0000E+00	F	cn0	.7418E-03	F	ayBias	-.5902E-01	F
cyBdot	.0000E+00	F	cnb	.2135E-02	F	pdotBias	.0000E+00	F
cyp	.0000E+00	F	cnb3	.0000E+00	F	rdotBias	.0000E+00	F
cyr	.0000E+00	F	cnBdot	.0000E+00	F	kb	1.640	F
cyda	.7661E-03	F	cnp	-.5000E-01	F	xb	-32.16	F
cydr	.3829E-02	F	cnr	-.2172	F	yb	.0000E+00	F
cyd3	-.8200E-04	F	cnda	.2827E-02	F	zb	-3.512	F
cyd4	.0000E+00	F	cndr	-.3189E-02	F	xay	-2.439	F
cl0	.8894E-02	F	cnd3	-.3800E-03	F	yay	-2.458	F
clb	-.1403E-02	F	cnd4	.0000E+00	F	zay	-1.437	F
clb3	.0000E+00	F	beta0	.0000E+00	F	gAlpha	.0000E+00	F
clBdot	.0000E+00	F	p0	.0000E+00	F	gQ	.0000E+00	F
clp	-.4295	F	r0	.0000E+00	F	gBeta	.0000E+00	F
clr	.1000	F	phi0	.0000E+00	F	gP	.0000E+00	F
clda	.2405E-02	F	betaBias	.0000E+00	F	gR	.0000E+00	F
cldr	-.1005E-02	F	pBias	.0000E+00	F			

APPENDIX D - SAMPLE LATERAL pEst OUTPUT

pEst:*Slanted text* represents user inputs. Units are defined in pEst manual [14].

pEst program for parameter estimation
Richard Maine/James Murray - NASA Dryden
version 2.3.4 10 Aug 90
this run date: time:

Help is available

pEst: *read m.p1f6e38c*

reading measured time history from file "m.p1f6e38c"
signal d1 not found. Using 0.
signal d2 not found. Using 0.
signal d4 not found. Using 0.
signal thrust not found. Using 0.

pEst: *restore c.p1f6e38c.final*

reading program status from file "c.p1f6e38c.final"

checking consistency of file "c.p1f6e38c.final" and file "m.p1f6e38c"

pEst: *states*

name	on?	limit	name	on?	limit
beta	T	.1000E+05	r	T	.1000E+05
p	T	.1000E+05	phi	T	.1000E+05

pEst: *resp*

name	weight	on?	name	weight	on?	name	weight	on?
beta	7.500	T	r	40.00	T	ay	1333.	T
p	4.400	T	phi	4.000	T			

pEst: *sho stats*

signal	average	signal	average	signal	average
de	-5.62	q	.223	ay	-.146E-01
d1	.000E+00	theta	8.14	pdot	-.268
d2	.000E+00	an	.990	rdot	-.807
da	-.452E-01	ax	-.154	qbar	164.
dr	-.225	qdot	1.16	mach	.340
d3	.332	beta	.662	thrust	.000E+00
d4	.000E+00	p	-.597	alt	.115E+04
v	378.	r	-.172		
alpha	10.4	phi	-.671		

pEst: *do mmle3.para*
reading from command file.

pEst: *par xa -25.5547*
name value on?

xa -25.55 F

pEst: *par ya .0000*
name value on?

ya .0000E+00 F

pEst: *par za -1.5037*
name value on?

za -1.504 F

pEst: *par xb -32.2380*
name value on?

xb -32.24 F

pEst: *par yb .0000*
name value on?

yb .0000E+00 F

pEst: *par zb -3.4954*
name value on?

zb -3.495 F

pEst: *par xax -2.6197*
name value on?

xax -2.620 F

pEst: *par yax -2.4308*
name value on?

yax -2.431 F

pEst: *par zax -1.4204*
name value on?

zax -1.420 F

pEst: *par xay -2.5172*
name value on?

xay -2.517 F

pEst: *par yay -2.4583*
name value on?

yay -2.458 F

pEst: *par zay -1.4204*
name value on?

zay -1.420 F

pEst: *par xan -2.6197*
name value on?

xan -2.620 F

pEst: *par yan -2.3617*
name value on?

yan -2.362 F

pEst: *par zan -1.4204*
name value on?

zan -1.420 F

pEst: *const ix 69022.4453*
name value

ix .6902E+05

pEst: *const iy 365324.0625*
name value

iy .3653E+06

pEst: *const iz 427141.6875*
name value

iz .4271E+06

pEst: *const ixz 4071.1189*
name value

ixz 4071.

pEst: *const mass 2250.4507*
name value

mass 2250.

pEst: *const xcg 0.0*
name value

xcg .0000E+00

pEst: *const ycg 0.0*
name value

ycg .0000E+00

pEst: *const zcg 0.0*
name value

zcg .0000E+00

pEst:
command file done.

pEst: *it 20*

name	value	on?	name	value	on?	name	value	on?
cy0	.6118E-02	T	clp	-.3053	T	cnb	.9239E-03	T
cyb	-.1737E-01	T	clda	-.1239E-02	T	cnr	-.1350	T
cydr	.6585E-02	T	cldr	.4348E-03	T	cndr	-.1094E-02	T
cl0	.1007E-02	T	cld3	-.4697E-03	T	cnd3	-.7729E-04	T
clb	-.1715E-02	T	cn0	-.6007E-03	T	ayBias	-.1430E-01	T

total cost = 45.80

cost per response :

beta	p	r	phi	ay
11.8	21.7	94.0	39.6	62.0

Iteration 1

Lev-Marq used 1 trials. v = .0000E+00 len = .1673 cost = 45.80

name	value	on?	delta	name	value	on?	delta
cy0	.6136E-02	T	.1819E-04	cld3	-.4696E-03	T	.6128E-07
cyb	-.1737E-01	T	.1348E-05	cn0	-.6001E-03	T	.5786E-06
cydr	.6586E-02	T	.6603E-06	cnb	.9233E-03	T	-.5162E-06
cl0	.1007E-02	T	.9192E-07	cnr	-.1347	T	.2231E-03
clb	-.1716E-02	T	-.7743E-06	cndr	-.1094E-02	T	.4461E-06
clp	-.3052	T	.9662E-04	cnd3	-.7735E-04	T	-.5351E-07
clda	-.1239E-02	T	-.4190E-06	ayBias	-.1433E-01	T	-.2753E-04
cldr	.4357E-03	T	.8805E-06				

total cost = 45.80

cost per response :

beta	p	r	phi	ay
11.8	21.7	94.1	39.5	61.9

iteration 1 used 19 integrations

** iteration converged

estimate used 19 integrations

pEst: *par all*

name	value	on?	name	value	on?	name	value	on?
cNorm0	.0000E+00	F	cmd2	.0000E+00	F	qBias	.0000E+00	F
cNorma	.1000	F	cmd3	.0000E+00	F	thetaBias	.0000E+00	F
cNorma2	.0000E+00	F	ca0	.0000E+00	F	anBias	.0000E+00	F
cNormAdot	.0000E+00	F	caa	.0000E+00	F	axBias	.0000E+00	F
cNormq	.0000E+00	F	caa2	.0000E+00	F	qdotBias	.0000E+00	F
cNormde	.5000E-02	F	caAdot	.0000E+00	F	ka	1.000	F
cNormde2	.0000E+00	F	caq	.0000E+00	F	xa	-25.55	F
cNormd1	.0000E+00	F	cade	.0000E+00	F	ya	.0000E+00	F
cNormd2	.0000E+00	F	cade2	.0000E+00	F	za	-1.504	F
cNormd3	.0000E+00	F	cad1	.0000E+00	F	xan	-2.620	F
cm0	.0000E+00	F	cad2	.0000E+00	F	yan	-2.362	F
cma	-.1000E-01	F	cad3	.0000E+00	F	zan	-1.420	F
cma2	.0000E+00	F	v0	.0000E+00	F	xax	-2.620	F
cmAdot	.0000E+00	F	alpha0	.0000E+00	F	yax	-2.431	F
cmq	-20.00	F	q0	.0000E+00	F	zax	-1.420	F
cmde	-.2000E-01	F	theta0	.0000E+00	F	xv	.0000E+00	F
cmde2	.0000E+00	F	vBias	.0000E+00	F	yv	.0000E+00	F
cmd1	.0000E+00	F	alphaBias	.0000E+00	F	zv	.0000E+00	F

name	value	on?	name	value	on?	name	value	on?
cy0	.6136E-02	T	cld3	-.4696E-03	T	rBias	.0000E+00	F
cyb	-.1737E-01	T	cld4	.0000E+00	F	phiBias	.0000E+00	F
cyb3	.0000E+00	F	cn0	-.6001E-03	T	ayBias	-.1433E-01	T
cyBdot	.0000E+00	F	cnb	.9233E-03	T	pdotBias	.0000E+00	F
cyp	.1884	F	cnb3	.0000E+00	F	rdotBias	.0000E+00	F
cyr	.3013	F	cnBdot	.0000E+00	F	kb	1.550	F
cyda	-.7500E-03	F	cnp	-.1956E-01	F	xb	-32.24	F
cydr	.6586E-02	T	cnr	-.1347	T	yb	.0000E+00	F
cyd3	-.8200E-04	F	cnda	-.1312E-03	F	zb	-3.495	F
cyd4	.0000E+00	F	cndr	-.1094E-02	T	xay	-2.517	F
cl0	.1007E-02	T	cnd3	-.7735E-04	T	yay	-2.458	F
clb	-.1716E-02	T	cnd4	.0000E+00	F	zay	-1.420	F
clb3	.0000E+00	F	beta0	.0000E+00	F	gAlpha	.0000E+00	F
clBdot	.0000E+00	F	p0	.0000E+00	F	gQ	.0000E+00	F
clp	-.3052	T	r0	.0000E+00	F	gBeta	.0000E+00	F
clr	.1499	F	phi0	.0000E+00	F	gP	.0000E+00	F
clda	-.1239E-02	T	betaBias	.0000E+00	F	gR	.0000E+00	F
cldr	.4357E-03	T	pBias	.0000E+00	F			

APPENDIX E - LONGITUDINAL EQUATIONS OF MOTION

State vector	$x = (\alpha, q, \theta)$
Control vector	$u = (\delta_e)$
Observation vector	$z = (\alpha_m, q_m, \theta_m, a_{n_m}, a_{x_m}, \dot{q}_m)$

The nonlinear longitudinal state equations are :

$$\begin{aligned}
\dot{\alpha} &= q - \frac{\bar{q}SR}{mV}C_L + \frac{gR}{V}(\cos\theta\cos\alpha + \sin\theta\sin\alpha) \\
&\quad -\frac{TR}{mV}\sin\alpha \\
I_{yy}\dot{q} &= \bar{q}ScRC_m \\
\dot{\theta} &= \dot{\theta}_0 + q
\end{aligned}$$

The $\dot{\theta}_0$ term is included to allow for instrument biases.

The longitudinal observation equations are :

$$\begin{aligned}
\alpha_m &= \alpha_0 + K_\alpha(\alpha - \frac{x_\alpha}{V}q) \\
q_m &= q_0 + q \\
\theta_m &= \theta_0 + \theta \\
a_{n_m} &= a_{n_0} + \frac{\bar{q}S}{mg}C_N + \frac{x_{a_n}}{gR}\dot{q} + \frac{z_{a_n}}{R^2g}q^2 \\
a_{x_m} &= a_{x_0} - \frac{\bar{q}S}{mg}C_A + \frac{z_{a_x}}{gR}\dot{q} - \frac{x_{a_x}}{R^2g}q^2 + \frac{T}{mg} \\
\dot{q}_m &= \dot{q}_0 + \dot{q}
\end{aligned}$$

The $\alpha_0, q_0, \theta_0, a_{n_0}, a_{x_0}$ and $\dot{q}_0$ terms represent instrument biases.

The expansions of the longitudinal force and moment coefficients are :

$$
\begin{aligned}
C_N &= C_{N_0} + C_{N_\alpha}\alpha + C_{N_q}\frac{qc}{2VR} + C_{N_{\delta_e}}\delta_e \\
C_m &= C_{m_0} + C_{m_\alpha}\alpha + C_{m_q}\frac{qc}{2VR} + C_{m_{\delta_e}}\delta_e + C_{m_{\dot{\alpha}}}\frac{\dot{\alpha}c}{2VR} \\
C_A &= C_{A_0} + C_{A_\alpha}\alpha + C_{A_q}\frac{qc}{2VR} + C_{A_{\delta_e}}\delta_e \\
C_L &= C_N \cos\alpha - C_A \sin\alpha
\end{aligned}
$$

APPENDIX F - LATERAL EQUATIONS OF MOTION

State vector $x = (\alpha, \beta, p, q, r, \theta, \phi)$

Control vector $u = (\delta_a, \delta_e, \delta_r, \delta_{sp})$

Observation vector $z = (\alpha_m, \beta_m, p_m, q_m, r_m, \theta_m, \phi_m, a_{x_m}, a_{y_m}, a_{n_m})$

The nonlinear lateral-directional state equations are :

$$\begin{aligned}
\dot{\alpha} &= q - \frac{\bar{q}SR}{mV\cos\beta}C_L + \frac{gR}{V\cos\beta}(\cos\theta\cos\phi\cos\alpha + \sin\theta\sin\alpha) \\
&\quad - \tan\beta(p\cos\alpha + r\sin\alpha) - \frac{TR}{mV\cos\beta}\sin\alpha \\
\dot{\beta} &= \frac{g}{V}R(\cos\beta\cos\theta\sin\phi - \sin\beta(\cos\theta\cos\phi\sin\alpha - \sin\theta\cos\alpha)) \\
&\quad + p\sin\alpha - r\cos\alpha + \frac{\bar{q}S}{mV}RC_Y \\
\dot{p}I_x - \dot{q}I_{xy} - \dot{r}I_{xz} &= \bar{q}SbRC_l + (qr(I_y - I_z) + (q^2 - r^2)I_{yz} + pqI_{xz} - prI_{xy})/R \\
\dot{q}I_y - \dot{r}I_{yz} - \dot{p}I_{xy} &= \bar{q}SbRC_m + (pr(I_z - I_x) + (r^2 - p^2)I_{xz} + qrI_{xy} - pqI_{yz})/R \\
\dot{r}I_z - \dot{p}I_{xz} - \dot{q}I_{yz} &= \bar{q}SbRC_n + (pq(I_x - I_y) + (p^2 - q^2)I_{xy} + prI_{yz} - qrI_{xz})/R \\
\dot{\theta} &= \dot{\theta}_0 + q\cos\phi - r\sin\phi \\
\dot{\phi} &= \dot{\phi}_0 + p + \tan\theta(r\cos\phi + q\sin\phi)
\end{aligned}$$

The $\dot{\theta}_0$ and $\dot{\phi}_0$ are included to allow for instrument biases.

The lateral observation equations are :

$$\begin{aligned}
\alpha_m &= \alpha_0 + K_\alpha(\alpha - \frac{x_\alpha}{V}q + \frac{y_\alpha}{V}p) \\
\beta_m &= \beta_0 + K_\beta(\beta - \frac{z_\beta}{V}p + \frac{x_\beta}{V}r) \\
p_m &= p_0 + p \\
q_m &= q_0 + q
\end{aligned}$$

$$
\begin{aligned}
r_m &= r_0 + r \\
\theta_m &= \theta_0 + \theta \\
\phi_m &= \phi_0 + \phi \\
a_{x_m} &= a_{x_0} - \frac{\bar{q}S}{mg}C_A + (\frac{z_{a_x}}{gR}\dot{q} - \frac{y_{a_x}}{gR}\dot{r}) - \frac{x_{a_x}}{R^2 g}(q^2 + r^2) + \frac{T}{mg} \\
a_{y_m} &= a_{y_0} + \frac{\bar{q}S}{mg}C_Y + (\frac{x_{a_y}}{gR}\dot{r} - \frac{z_{a_y}}{gR}\dot{p}) - \frac{y_{a_y}}{R^2 g}(p^2 + r^2) \\
a_{n_m} &= a_{n_0} + \frac{\bar{q}S}{mg}C_N + (\frac{x_{a_n}}{gR}\dot{q} - \frac{y_{a_n}}{gR}\dot{p}) + \frac{z_{a_n}}{R^2 g}(q^2 + p^2) \\
\dot{p}_m &= \dot{p}_0 + \dot{p} \\
\dot{q}_m &= \dot{q}_0 + \dot{q} \\
\dot{r}_m &= \dot{r}_0 + \dot{r}
\end{aligned}
$$

The $\alpha_0, \beta_0, p_0, q_0, r_0, \theta_0, \phi_0, a_{x_0}, a_{y_0}, a_{n_0}, \dot{p}_0, \dot{q}_0$ and $\dot{r}_0$ terms represent instrument biases.

The expansions of the lateral force and moment coefficients are :

$$
\begin{aligned}
C_Y &= C_{Y_0} + C_{Y_\beta}\beta + C_{Y_p}\frac{pb}{2VR} + C_{Y_r}\frac{rb}{2VR} + C_{Y_\delta}\delta \\
C_l &= C_{l_0} + C_{l_\beta}\beta + C_{l_p}\frac{pb}{2VR} + C_{l_r}\frac{rb}{2VR} + C_{l_\delta}\delta + C_{l_{\dot{\beta}}}\frac{\dot{\beta}b}{2VR} \\
C_n &= C_{n_0} + C_{n_\beta}\beta + C_{n_p}\frac{pb}{2VR} + C_{n_r}\frac{rb}{2VR} + C_{n_\delta}\delta + C_{n_{\dot{\beta}}}\frac{\dot{\beta}b}{2VR}
\end{aligned}
$$

where the δ terms are summed over all controls.

$$
\begin{aligned}
C_{Y_\delta}\delta &= C_{Y_{\delta_a}}\delta_a + C_{Y_{\delta_r}}\delta_r + C_{Y_{\delta_{sp}}}\delta_{sp} \\
C_{l_\delta}\delta &= C_{l_{\delta_a}}\delta_a + C_{l_{\delta_r}}\delta_r + C_{l_{\delta_{sp}}}\delta_{sp} \\
C_{n_\delta}\delta &= C_{n_{\delta_a}}\delta_a + C_{n_{\delta_r}}\delta_r + C_{n_{\delta_{sp}}}\delta_{sp}
\end{aligned}
$$

DISTRIBUTION

AUSTRALIA

Defence Organisation

Defence Science and Technology Organisation

Chief Defence Scientist
FAS, Science Policy
AS, Science Corporate Management
AS, Science Industry Interaction
} (shared copy)

Counsellor, Defence Science, London (Doc Data sheet only)
Counsellor, Defence Science, Washington (Doc Data sheet only)
Scientific Adviser to Thailand MRD (Doc Data sheet only)
Scientific Adviser to the DRC (Kuala Lumpur) (Doc Data sheet only)
Senior Defence Scientific Adviser/Scientific Adviser Policy and Command (shared copy)
Navy Scientific Adviser (Doc Data sheet only)
Scientific Adviser - Army (Doc Data sheet only)
Air Force Scientific Adviser
Director Trials

Aeronautical and Maritime Research Laboratory

Director
Chief of Air Operations Division
Research Leader - Aircraft Performance
Head, Air Surface Operations
Author: A. D. Snowden
Author: J. S. Drobik
G. J. Brian
R. A. Stuckey

DSTO Library

Library, Fishermens Bend
Library, Maribyrnong
Main Library DSTOS (2 copies)
Library, MOD, Pyrmont (Doc Data sheet only)

Defence Central

OIC TRS, Defence Central Library
Officer in Charge, Document Exchange Centre, 1 copy
US Defence Technical Information Centre, 2 copies
UK Defence Research Information Centre, 2 copies
Canada Defence Scientific Information Service, 1 copy
NZ Defence Information Centre, 1 copy
Defence Intelligence Organisation
Library, Defence Signals Directorate (Doc Data sheet only)

HQADF

DD-OFFOPS, Canberra

Air Force

Logistics Systems Agency
Director, Technical Airworthiness
ATS-3
F-111C Mission Simulator Project
RESSIMENG
Aircraft Research and Development Unit
OC ARDU
CO Flight Test Squadron
ASCENG
Library
RAAF Base Amberley
OC 82 Wing
CO, 1 Sqn
CO, 6 Sqn
OIC ATF ATS, RAAFSTT, WAGGA (2 copies)

Army

Director General Force Development (Land) (Doc Data sheet only)
ABCA Office, G-1-34, Russell Offices, Canberra (4 copies)
SO (Science), HQ 1 Division, Milpo, Enoggera, Qld 4057 (Doc Data sheet only)
NAPOC QWG Engineer NBCD c/- DENGRS-A, HQ Engineer Centre
Liverpool Military Area, NSW 2174

SPARES (5 copies)

AL 149 DEPARTMENT OF DEFENCE

DOCUMENT CONTROL DATA

PAGE CLASSIFICATION

UNCLASSIFIED

PRIVACY MARKING

1a. AR NUMBER	1b. ESTABLISHMENT NUMBER	2. DOCUMENT DATE	3. TASK NUMBER
AR-009-660	DSTO-TR-0321	APRIL 1996	94/205

4. TITLE

F-111C LONGITUDINAL AND LATERAL AERODYNAMIC FLIGHT DATA ANALYSIS FOR TAKE-OFF AND LANDING CONFIGURATIONS

5. SECURITY CLASSIFICATION (PLACE APPROPRIATE CLASSIFICATION IN BOX(S) IE. SECRET (S), CONF. (C) RESTRICTED (R), LIMITED (L), UNCLASSIFIED (U)).

DOCUMENT	TITLE	ABSTRACT
U	U	U

6. NO. PAGES: 72

7. NO. REFS.: 28

8. AUTHOR(S)

A.D. Snowden
J.S. Drobik

9. DOWNGRADING/DELIMITING INSTRUCTIONS

Not applicable.

10. CORPORATE AUTHOR AND ADDRESS

AERONAUTICAL AND MARITIME RESEARCH LABORATORY
AIR OPERATIONS DIVISION
PO BOX 4331
MELBOURNE, VIC 3001, AUSTRALIA

11. OFFICE/POSITION RESPONSIBLE FOR:

DTA-LSA

SPONSOR CAOD

SECURITY CAOD

DOWNGRADING CAOD

APPROVAL

12. SECONDARY DISTRIBUTION (OF THIS DOCUMENT)

Approved for public release.

OVERSEAS ENQUIRIES OUTSIDE STATED LIMITATIONS SHOULD BE REFERRED THROUGH DOCUMENT EXCHANGE CENTRE, DIS NETWORK OFFICE, DEPT OF DEFENCE, CAMPBELL PARK OFFICES, CANBERRA ACT 2600.

13a. THIS DOCUMENT MAY BE ANNOUNCED IN CATALOGUES AND AWARENESS SERVICES AVAILABLE TO ....

No Limitations.

14. DESCRIPTORS

Computerised simulation
F-111C aircraft
Flight dynamics
[illegible]
System identification

15. DISCAT SUBJECT CATEGORIES

16. *ABSTRACT*

A series of flight trials was performed on an F-111C aircraft, tail number A8-132, at the RAAF's Aircraft Research and Development Unit. Data obtained from the tests has been analysed in Air Operations Division to determine the aircraft aerodynamic and control derivatives. In this report the longitudinal and lateral derivatives for the take-off and landing configurations are presented and compared with wind tunnel results.

PAGE CLASSIFICATION
UNCLASSIFIED
PRIVACY MARKING

THIS PAGE IS TO BE USED TO RECORD INFORMATION WHICH IS REQUIRED BY THE ESTABLISHMENT FOR ITS OWN USE BUT WHICH WILL NOT BE ADDED TO THE DISTIS DATA UNLESS SPECIFICALLY REQUESTED.

16. ABSTRACT (CONT).

17. IMPRINT

AERONAUTICAL AND MARITIME RESEARCH LABORATORY, MELBOURNE

18. DOCUMENT SERIES AND NUMBER	19. WA NUMBER	20. TYPE OF REPORT AND PERIOD COVERED
DSTO Technical Report	71740C	

21. COMPUTER PROGRAMS USED

pEst
EXTRACT
FDP

22. ESTABLISHMENT FILE REF.(S)

M1/9/60

23. ADDITIONAL INFORMATION (AS REQUIRED)